This is to certify that the
thesis entitled

CFD SIMULATION OF TWO-PHASE FLOWS
IN A VERTICAL DUCT

presented by

Iffat Tasneem Shaik Mohammad

has been accepted towards fulfillment
of the requirements for the

Master of Science degree in Mechanical Engineering

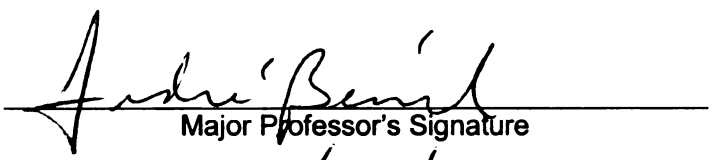

Major Professor's Signature

2/26/06

Date

CFD SIMULATION OF TWO-PHASE FLOWS IN A VERTICAL DUCT

By

Iffat Tasneem Shaik Mohammad

A THESIS

Submitted to
Michigan State University
in partial fulfillment of the requirements
for the degree of

MASTER OF SCIENCE

Department of Mechanical Engineering

2006

ABSTRACT

CFD SIMULATION OF TWO-PHASE FLOWS IN A VERTICAL DUCT

By

Iffat Tasneem Shaik Mohammad

The flow of a suspension of spherical particles in air through a vertical rectangular channel with equal inlet and outlet cross sectional areas was simulated under isothermal conditions using Fluent. An Eulerian approach was used in which the multiphase problem is represented as two interpenetrating continua. A granular model was employed for the mixture stress and a realizable "eddy" viscosity model was used for the Reynolds stress. The purpose of this work was to evaluate the ability of the multiphase model to capture the flow physics associated with catalytic risers. Experimental findings of Ibsen et al. (2001) were used for evaluating the numerical predictions. The numerical predictions were able to capture the axial and span wise particle velocity in some regions of the flow but failed to capture the correct pressure drop. In addition, while the turbulence model provided realizable results for the single-phase flows tested, it became unrealizable when coupled with the multiphase granular model.

To my husband, daughter and parents.

ACKNOWLEDGEMENTS

First and foremost, I would like to thank Almighty ALLAH for everything in my life. My heartfelt thanks to my parents for everything they did for me; their generous support, motivation and trust in me since childhood, which helped me aim higher from time to time. Great thanks to my wonderful husband and beautiful daughter for all the love and patience and for being a constant source of inspiration. Thanks to my sister and brother for their moral support. Thanks also to all my relatives whose confidence in me further encouraged my performance and betterment.

I sincerely thank my advisor Dr. Andre Benard, who helped me work in the area of my research interest - Computational Fluid Dynamics and for all his support and guidance throughout my Master's. His training, advice and insight into things have been invaluable.

I would like to thank Dr. Kuochen Tsai from Dow chemicals for suggesting this interesting and challenging research topic. Thanks to Dr. Charles Petty and Dr. Farhad Jaberi, for being on the committee and for their invaluable suggestions. A special thanks to all the professors at MSU for being there for me at all times. Thanks to my team mates Deep and Karuna for their invaluable assistance on our summer workshop project.

For technical assistance I would like to thank Kapil Das Sahu from FLUENT (India) for his immense help all along my Master's. I would also like to thank Andrew Keen for helping me get going smoothly with parallel computing.

Finally, I gratefully acknowledge the financial support of this work by the NSF I/UCRC-MTP.

TABLE OF CONTENTS

LIST OF TABLES

LIST OF FIGURES

NOMENCLATURE

D_h	Hydraulic diameter [m]
C_D	Drag coefficient [dimensionless]
f	Drag function [dimensionless]
X,Y,Z	Coordinates [m]
D	Depth of riser [m]
H	Riser height [m]
W	Width of riser [m]
V	Volume [m^3]
dV	Variation in volume [m^3]
d_p	Particle diameter [m]
dz	Dimensions of measurement length [m]
dp	Variation in pressure [Pa]
e	Restitution coefficient
G_s	Solids flux [kg/m^2s]
$\vec{g}$	Gravitational acceleration [m/s^2]
$g_{0,ss}$	Radial distribution coefficient
m_s	Mass of solid [kg]
N_{cell}	Number of grid cells [dimensionless]
p	Pressure [Pa]
p_s	Solid phase pressure [Pa]
t	Time [s]
Re	Reynolds number [dimensionless]
Re_s	Solid Reynolds number [dimensionless]
$\bar{\bar{S}}$	Mean rate-of-strain tensor [s^{-1}]
$\vec{u}$	Axial velocity component [m/s]
$\vec{v}$	Span wise velocity component [m/s]
$\vec{w}$	Span wise velocity component [m/s]
x/H	Dimensionless height [dimensionless]
y/D	Dimensionless depth [dimensionless]
z/W	Dimensionless width [dimensionless]
N, n	Numbers
$\bar{\bar{I}}$	Identity matrix [dimensionless]
$\overline{\vec{u}_i'\vec{u}_j'}$	Reynolds stress
G	Generation
Y	Dissipation
D	Material derivative
x	Displacement

Greek symbols

∂	Local derivative
γ	Dissipation of turbulent kinetic energy by collision [kg/ms3]
δ	Kronecker delta [dimensionless]
α	Volume fraction [dimensionless]
k	Transport coefficient of turbulent kinetic energy [kg/ms]
μ	Dynamic Viscosity [Pa-s]
ν	Kinematic viscosity [m^2/s]
ϕ	Energy exchange between two phases [J/kg]
$\bar{\nu}$	Modified turbulent viscosity [m^2/s]
ρ	Density [kg/m3]
$\bar{\bar{\tau}}$	Shear stress [Pa]
τ_p	Particle relaxation time [s]
Ω	Angular velocity, Mean rate of rotation tensor [s^{-1}]
ε	Turbulent dissipation rate [m^2/s^3]
ω	Specific dissipation rate [s^{-1}]
π	Constant [dimensionless]
λ	Eigen values [dimensionless]
K	Interphase exchange coefficient [dimensionless]
$\hat{\rho}$	Effective density [kg/m3]
σ	Prandtl number [dimensionless]

Subscripts

g	Gas
k	Phase number
s	Solid
q	Primary phase
p	Liquid
t	Turbulent
k	Turbulent kinetic energy[kg/ms]
ε	Turbulent dissipation rate [m^2/s^3]

Superscripts

T	Transpose

CHAPTER 1

INTRODUCTION

1.1 Introduction to Circulating Fluidized Bed

The study of multiphase flows represents a challenging and fruitful area of endeavor since the state of the art for multiphase flows is considerably more primitive where the correct formulation of the governing equations is still under debate whereas the transport equations of single phase Newtonian fluids are generally well-accepted and closed form solutions for specific cases are well documented.

Numerical simulation of flows associated with risers is the main topic of this thesis. Gas-solids fluidization has a wide application in chemical, metallurgical and energy industries with the largest applications being in fluidized bed reactors in coal combustion for large scale thermoelectric power generation and catalytic cracking of petroleum to produce gasoline and other fuels. The use of circulating fluidized bed system is increasing as it can be applied to a wide area of applications such as power generation, catalytic cracking and drying of wet powders with a good result (low cost to performance ratio). The circulating fluidized bed combustors are superior to pulverized coal combustors regarding fuel flexibility and emission performance of NO_x and SO_2.

An advantage of circulating fluidized bed combustor is that it can be fired with low-grade coal, biomass and waste with reasonable efficiency whereas its disadvantage being the emission of small particle. Hence, it is necessary to put energy into separating the particles from the outflow. Today several hundreds of circulating fluidized bed combustors is operating with the largest ones delivering 250 MW of power.

One of the possible reasons for the rather modest maximal turn out of power is the lack of good design tools for scale-up of the process. Computational Fluid Dynamics (CFD) software has proven to be a relatively efficient tool for design of applications with single-phase flows. However, for multiphase flow, CFD models still need to be improved before the same precision in the results can be obtained. This study will focus on simulating a multiphase problem with the purpose of assessing the accuracy of the simulations through a realizability diagram.

The structure of multiphase flows in circulating fluidized bed columns is quite complex, showing great variations on solids volumetric fraction throughout the riser, involving continuous formation and dissipation of clusters, and a high rate of recirculation of solids leading to an intense superficial contact between gas and solids providing high reaction rates. Therefore, the knowledge of the flow hydrodynamics is of great importance, allowing relevant reactive and mass transport parameters to be determined.

The mathematical modeling of gas-solids fluidization processes represents an ancillary tool for minimizing the experimental efforts required for developing industrial plants. However, mathematical modeling and numerical simulation are in continuous development, contributing in a growing way for the better understanding of processes and physical phenomena. Mathematical models require experiments in order to be validated and, concerning fluidization, the required experiments involve complex measurements. Hence, mathematical modeling also represents an incentive for the development of new experimental methods and techniques.

In this work, numerical simulations are performed for the gas-solids flow in a riser of circulating fluidized bed using the Eddy Viscosity Model proposed by Shih et al. (1995).

1.2 Principles of a Circulating Fluidized Bed

A Circulating Fluidized Bed schematic is as shown in Figure 1.1.

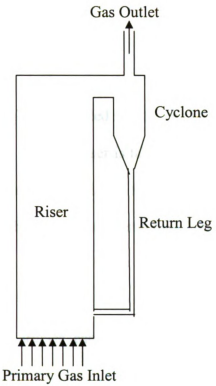

Figure 1.1: Schematic of a Circulating Fluidized Bed

It consists mainly of a riser, a cyclone and a return leg. In the riser, particles that form a particulate bed in the bottom are kept in free motion by an upward flowing gas (or liquid) hence the term "fluidized bed". When the superficial gas velocity is sufficiently high the particles will rise to the exit of the riser and enter the cyclone. A cyclone is used to separate the particles from the out flowing gas. The separated particles are then reintroduced into the riser through the return leg, hence the term "circulating". As the

superficial gas velocity increases from zero the system goes through fixed bed, bubbling regime, slug flow, turbulent regime and finally in the fast fluidization regime. The flows studied in this thesis are associated to a circulating fluidized bed operated in the turbulent and the fast fluidization regime.

1.3 Previous work in the area of Circulating Fluidized Bed

In the following subsections previous work in the field of experimental and numerical analysis of gas-solid flow will be discussed.

1.3.1 Experimental work

Circulating fluidized beds can roughly be divided into two categories based on the layout of the riser: The fluidized catalytic cracking riser is tall with a height to width ratio well above 10 and most often cylindrical; the circulating fluidized bed combustor riser which is low with a height to width ratio below 10 and mostly based on a square sectioned. The gas-particle flows experienced in these two types of risers differ as a result of the difference in the layout.

In the literature, various articles can be found on experimental findings in circulating fluidized beds. Two types of non-intrusive measuring devices, based upon laser light have been used in the past for obtaining experimental results namely the Laser/Phase Doppler Anemometry and the Particle Image Velocimetry. Zhang et al. (1995), Werther et al. (1996), Samuelsberg et al.(1996), Wang et al. (1998) and Mathiesen et al. (2000) obtained experimental results in circulating fluidized bed of the first category of risers using Laser Doppler Anemometry. Laser Doppler Anemometry was also used by Berkelmann et al. (1991), Wang et al. (1993), Van den Moortel et al. (1997), and Zhou et al. (2000) to obtain experimental results in circulating fluidized bed

of the second category of risers. The circulating fluidized bed investigated by Berkelmann et al. (1996) was a 4 MW fluidized bed combustor whereas the remaining references investigated laboratory scale models. Gidaspow et al. (1992) measured solids flux with a sampling probe and solids concentration with an X-ray probe. From the solids flux and the solids concentration they deduced the solids velocity. Werther et al. (1997) measured solids volume concentrations and solids velocities with a guarded capacitance probe in a 109 MW circulating fluidized bed boiler at full load.

All the references mentioned above deal with the properties of the solids in a circulating fluidized bed. References concerning measurements of both gas and solid velocities are scarce but existent. Hamdullahpur et al. (1987) measured gas, and two different solid phases present in a laboratory scale circulating fluidized bed boiler model. Yang et al. (1993) measured gas and solids velocities in a fluidized catalytic cracking riser with a Laser Doppler Anemometry system under relatively dilute operating conditions. The gas flow was seeded with talcum particles (d_p = 1 μ m). (Bensalah 1999) used a Phase Doppler Anemometry system for measuring both phases in a circulating fluidized bed test rig which was operated under relatively dilute conditions. Glass particles with two non-overlapping particle size distributions were used for the gas and solid phase, respectively, thereby distinguishing the two phases by their sizes. The mean diameter for the seeding glass particles was 9 μ m and the mean diameter for the solids was 60 μ m. Gillandt et al. (2001) measured gas and solid properties in a particle laden jet with a particle range of 1:200 with a Phase Doppler Anemometry system.

1.3.2 Numerical simulations

Numerical predictions of multiphase flow by CFD models have gained a more widespread use over the past years. When narrowing the multiphase flow field into gas-particle flows there exists two different CFD approaches namely the Eulerian-Lagrangian and the Eulerian–Eulerian. In this thesis, attention will be put on the latter CFD approach. When modeling the gas-particle flow with an Eulerian multiphase model it has become more and more customary to rely on the kinetic theory of granular flow for modeling the particle phase.

The theory of the model is based on kinetic theory of non-uniform gasses, as presented by Chapman et al. (1970). The model was developed and matured through publications as Jenkins et al.(1983), Lun et al.(1984), Jenkins et al. (1987), Gidaspow et al.(1990) and Gidaspow (1994). A wide variety of models have been used ranging from very simple approaches solving only the basic equations to more advanced approaches solving a large number of equations.

Sundaresan et al. (1991), Nieuwland et al. (1996), Samuelsberg et al.(1996), Mathiesen et al.(1999) and Neri et al.(2000) made numerical predictions with a two-dimensional two-phase numerical model of a vertical riser section of a circulating fluidized bed. Gidaspow et al. (1992), Samuelsberg et al. (1996), Mathiesen et al. (2000) simulated the entire fluidized bed including cyclone and return leg in two dimensions. Sun et al. (1999) and Benyahia et al. (2000) made two-dimensional two-phase simulations of circulating fluidized bed riser flow for the participation in the PSRI challenge problem (1995) presented at the Fluidization XIII conference.

Expanding the numerical model from two to three dimensions has the clear advantage of including three-dimensional effects in the numerical predictions. A disadvantage is the considerable increase in the size of the problem, which needs to be solved. Benyahia et al. (1999) predicted the flow in a tall cylindrical riser in three dimensions using fluidized catalytic cracking particles for the solid phase. Kuipers et al. (1999), Mathiesen et al. (1999) predicted gas-particle flow in a circulating fluidized bed with a square sectioned riser in three dimensions and found the largest average concentration of solids in the corners of the riser. Balzer et al. (1997) predicted the flow in an industrial circulating fluidized bed boiler of 125MW with a three-dimensional model using 350,000 nodes. The model was based on a comprehensive set of equations related to the kinetic theory of granular flow approach. De Wilde et al. (2001) also used a comprehensive model with a large number of equations to predict the flow in a cylindrical fluidized catalytic cracking riser in three dimensions. Zhang et al. (2001) predicted the flow in a fluidized bed riser with a simple model solving a small number of equations but used a relatively large number of grid cells for the numerical simulation. The Euler/Lagrange approach has most often been used for predicting the flow in bubbling gas-fluidized beds (e.g. Hoomans et al. (1996), Hoomans et al. (2000), van Wachem et al. (2001), but has also been used for predicting the flow in the riser of a circulating fluidized bed (e.g. Helland et al. (2000), Helland et al. (2002). (Helland et al. (2000) simulated fluidized bed riser flow in two dimensions with an Euler/Lagrange model tracking 250,000 particles.

The numerical modeling of bubbling fluidized beds are related to the modeling of circulating fluidized beds. In the area of bubbling fluidized beds, interesting work has

appeared which can inspire the improvement of circulating fluidized bed modeling. Syamlal (1998) modeled a bubbling fluidized bed and compared a first order upwind scheme with second order schemes for discretizing the convection terms and found that more realistic results were obtained with the second order schemes. Enwald et al. (1999) evaluated four different closures of the two-dimensional form of the Euler/Euler model, with and without gas and particulate-phase turbulence models. Additionally, they evaluated a two-dimensional model with the simplest closure on a refined mesh and concluded that it was of higher priority to carry out the calculations on a fine mesh than to use more sophisticated models.

1.4 Objectives of the thesis

The overall objective of this work is to evaluate the usage of single phase and two-phase turbulent models using CFD code FLUENT 6.2. in their ability to capture the important physical phenomena encountered in a riser by comparing the numerical predictions against the experimental findings of Ibsen et al.(2001).

These objectives are achieved through the following four tasks.

1. Verification of fully developed single phase laminar flow in a channel.
2. Realizability of various turbulent viscous models.
3. Comparison of various drag interphase models in a bubbly flow.
4. Verification and realizability of multiphase models in gas-solid simulations.

1.5 Computational domain considered in this work

The computational domain considered in all the simulations is as shown in Figure 1.2.

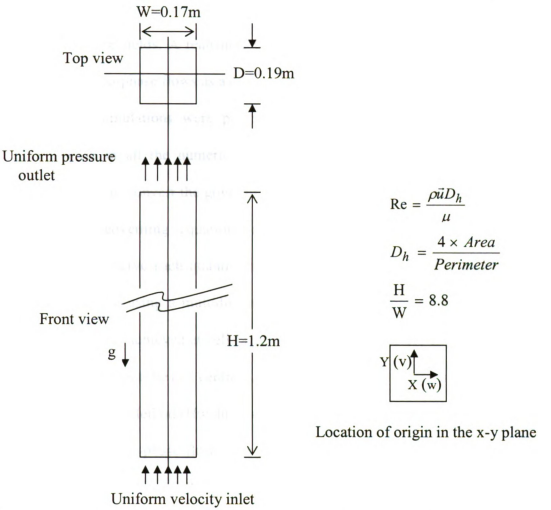

Figure1.2: Geometry of 3D-vertical upward channel flow considered in the simulation

As the geometry considered here is rectangular, a three dimensional Cartesian geometry is chosen with dimensions 0.17 x 1.20 x 0.19m, width(x) x height (y) x depth (z) respectively, in order to match with the experimental device (Ibsen et al., 2001). A staggered "hex-cooper" volume mesh was created in GAMBIT 2.2 with a very fine mesh near the walls and a rather coarse mesh at the center. The grid is made of 146,880 cells and 156,695 nodes (35, 37 and 121 nodes in x, y and z directions respectively).

1.6 Theoretical and Numerical considerations of this work

The numerical simulations involve solving the Reynolds Averaged Navier-Stokes (RANS-) equation and the Reynolds averaged continuity equation for the mean velocity and mean pressure fields. A realizable eddy viscosity model for the Reynolds stress is used in case of two-phase flows as a closure for the RANS-equation.

All the simulations were performed using a segregated solver. The upwind scheme is used in all the numerical simulations in which the control-volume based technique is used to convert the governing equations to algebraic equations consisting of integrating the governing equations about each control volume, yielding discrete equations that conserve each quantity on a control-volume basis. The quantities at cell faces are computed using a multidimensional linear reconstruction approach where the order of accuracy is achieved at cell faces through a Taylor series expansion of the cell-centered solution about the cell centroid. The set of algebraic equation is solved using the Algebraic Multigrid Method (Hutchinson et al., 1986)

In case of two-phase flows, the Eulerian multiphase model was used where the coupling is achieved through the pressure and interphase exchange coefficients using the Phase Coupled SIMPLE algorithm for the pressure-velocity coupling, (Patankar, 1980).

1.7 Boundary and Initial Conditions applied in this work

The geometry of the physical domain and the boundary conditions are shown in Figure 1.2.

For single phase simulations: On the bottom side of the riser, an upward uniform velocity was specified; on the lower side, the pressure relative to a reference pressure was specified as zero. The simulation imposes a no slip condition at the wall.

For two-phase simulations: In addition to the above conditions, the volume fraction of the dispersed phase on the inflow boundary was specified. The velocity of the primary phase and the velocity of the secondary phase were assumed equal and uniform. A zero backflow volume fraction was specified for the dispersed phase on the pressure patch.

Initial conditions for single-phase simulations: Zero initial velocity was specified in the flow domain for all the single-phase simulations.

Initial conditions for two-phase simulations: The initial concentration of the secondary phase was zero in the flow domain for all the two-phase simulations.

CHAPTER 2

SINGLE PHASE FLOW

2.1 VERIFICATION OF FULLY DEVELOPED LAMINAR FLOW IN A DUCT

The objective of this section is to perform the numerical simulation of a fully developed laminar flow in a channel and to validate the computational results by comparing the span wise velocities against the analytical solution as given in equation (2.3). The simulations were performed by considering air as a Newtonian fluid (constant ρ and constant μ) with a Reynolds number of 5 based on hydraulic diameter. The steady state grid independent numerical predictions of span wise velocities are compared with the analytical solution and the error in the numerical predictions has been computed.

2.1.1 Governing equations applied to laminar single phase simulations

The governing equations used in this simulation are as follows

Continuity Equation

$$\nabla \cdot \vec{U} = 0 \tag{2.1}$$

The conservation of momentum is

$$\left(\vec{U} \cdot \nabla\right) \vec{U} = -\frac{\nabla p}{\rho} + \nu \nabla^2 \vec{U} + \vec{g} \tag{2.2}$$

where ρ, ν and $\vec{U}$ are the density, kinematic viscosity and velocity of the fluid respectively. $\vec{g}$ is the acceleration due to gravity and p is the static pressure.

2.1.2 Analytical solution for fully developed single phase channel flow

For a fully developed single phase laminar flow in a square cross-section, the analytical solution is given by Constantinescu V. N. (1995) and in Handbook of Physics (2002).

$$\vec{U} = -\frac{16\left(\frac{W}{2}\right)^2}{\pi^3 \mu}\frac{dp}{dz}\sum_{n=1,3,5}^{\infty}(-1)^{(n-1)/2}\left[1-\frac{\cosh(n\pi Y/W)}{\cosh(n\pi D/2W)}\right]\frac{\cos(n\pi X/W)}{n^3} \qquad (2.3)$$

where W and D are the width and depth of the square channel.

2.1.3 Numerical results and verification

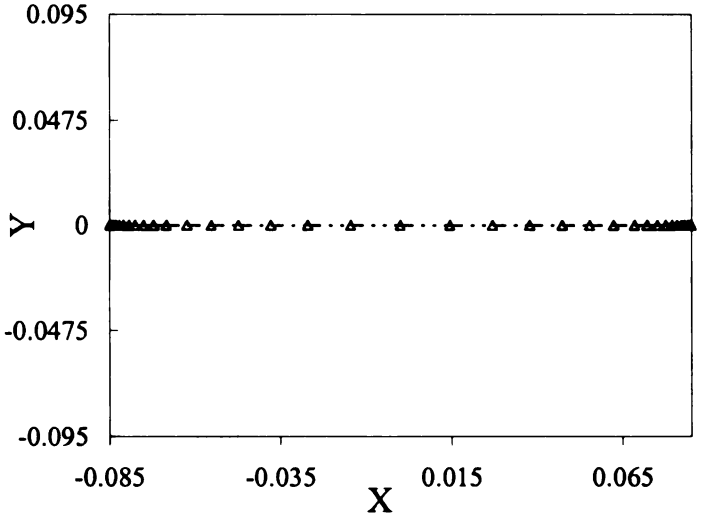

Figure 2.1: Plot of location of points at which the velocity profiles are drawn for Z/H = -0.8.

Figure 2.1 shows the location at which a comparison between the numerical and analytical span wise velocities is made in Figure 2.2 at an axial location of 1m. above the bottom of the riser. The numerical predictions compares very well with the analytical solution except near the centerline which exhibits a small error. Figure 2.3 shows the absolute error in the numerical results. It can be seen that the maximum error of 1.4E-05 is found at the centerline. This could be due to numerical errors encountered in the calculations. The error is calculated as

Absolute error calculation: Analyticalvalue – Numerical value

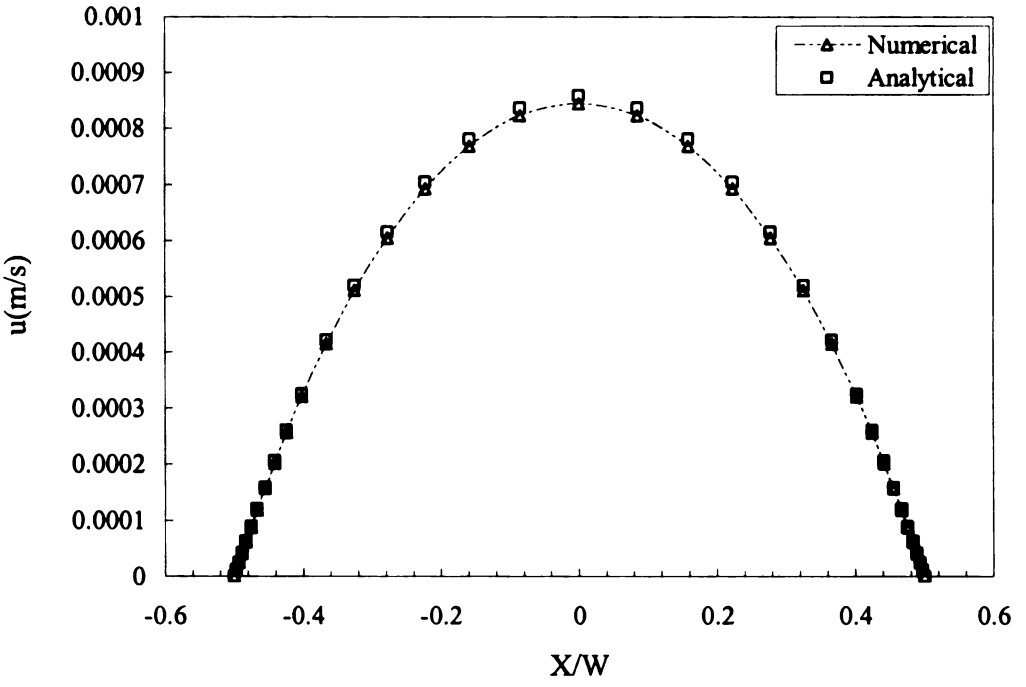

Figure 2.2: Plot of comparison of numerical and analytical span wise velocities. They predict almost the same with a slight error. See pg 13 for error calculation

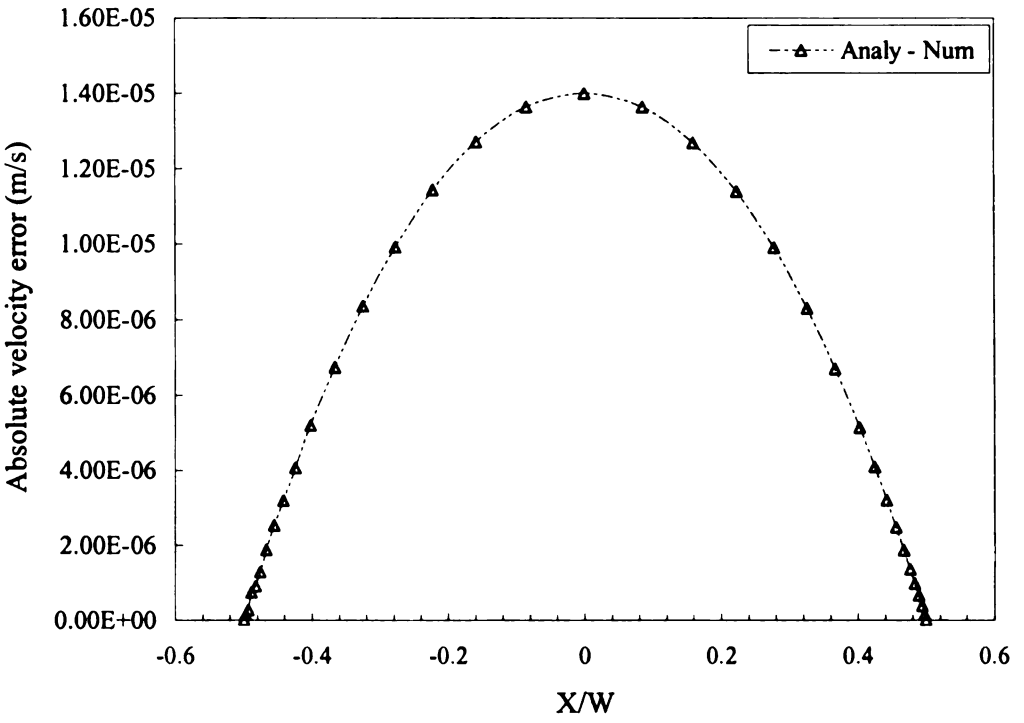

Figure 2.3: Plot of absolute velocity error vs. dimensionless width. A maximum absolute error of 1.4E-05 was found at the centerline.

2.2 COMPARISON OF VARIOUS VISCOUS MODELS IN A TURBULENT DUCT FLOW

2.2.1 Governing equations applied to turbulent single phase simulations

The actual or instantaneous velocity is decomposed into mean $\vec{u}$ and fluctuating velocities $\vec{u}'$ as

$$\vec{U} = \vec{u} + \vec{u}' \tag{2.4}$$

The continuity equation applied to $\vec{u} + \vec{u}'$ then gives

$$\nabla \cdot \vec{U} = 0 \tag{2.5}$$

The conservation of momentum applied to the averaged field gives

$$\rho(\vec{u} \cdot \nabla \vec{u}) = -\nabla p + \mu \nabla^2 \vec{u} + \rho \vec{g} - \rho \nabla \cdot [\overline{\vec{u}'\vec{u}'}] \tag{2.6}$$

where ρ, μ and $\vec{u}$ are the density, viscosity and velocity of the fluid respectively. $\vec{g}$ is the acceleration due to gravity and p is the static pressure.

Ensemble averaging is used to extract the mean flow properties from the instantaneous ones as $u_i(\vec{x},t) = \lim_{N\to\infty} \frac{1}{N} \sum_{n=1}^{N} u_i^{(n)}(\vec{x},t)$ (2.7)

$$U_i(\vec{x},t) = u_i(\vec{x},t) + u_i'(x',t) \tag{2.8}$$

The Reynolds-averaged momentum equation is

$$\rho\left(u_j \frac{\partial u_i}{\partial x_j}\right) = -\frac{\partial p}{\partial x_i} + \frac{\partial}{\partial x_j}\left(\mu \frac{\partial u_i}{\partial x_j}\right) + \frac{\partial R_{ij}}{\partial x_j} + \rho \vec{g} \tag{2.9}$$

where $R_{ij} = -\rho \overline{\vec{u}_i' \vec{u}_j'}$ is called the Reynolds stress. The Reynolds stress components have additional unknowns introduced by the averaging procedure, hence they must be modeled (related to the averaged flow quantities) in order to close the equations and this can be done in one of the following ways:

1. **Eddy-Viscosity Models** (Boussinesq, 1877).

It is a mathematical analogy to the stress-rate-of-strain relation for a Newtonian fluid. According to this hypothesis, the Reynolds stresses are modeled using an eddy (or turbulent) viscosity μ_t as

$$R_{ij} = -\rho\overline{u_i'u_j'} = \mu_t\left(\frac{\partial u_i}{\partial x_j} + \frac{\partial u_j}{\partial x_i}\right) - \frac{2}{3}\left(\rho k + \mu_t \frac{\partial u_i}{\partial x_i}\right)\delta_{ij} \tag{2.10}$$

2. Reynolds Stress Model (Gibson et al., 1978); (Launder, 1989); (Launder et al., 1975).

It involves calculation of the individual Reynolds stress components, $\overline{\vec{u}_i'\vec{u}_j'}$ using differential transport equations. The individual Reynolds stress components are then used to obtain closure of the Reynolds-averaged momentum equation. The exact form of the Reynolds stress transport equations may be derived by taking moments of the exact momentum equation. This is a process wherein the exact momentum equations are multiplied by a fluctuating property, the product then being Reynolds-averaged.

The scope of this section is to verify the realizability of various viscous models used in Fluent 6.2 namely the Spalart-Allmaras, the Standard k-ω, the Realizable k-ε and the Reynolds Stress Model. The steady state numerical simulations of a turbulent single phase flow in a channel were performed by considering air as a Newtonian fluid with a Reynolds number of 10,000 based on hydraulic diameter. The near wall treatment specifications can be found in Appendix A. The eigenvalues of the Reynolds stress term $-\rho\overline{u_i'u_j'}$ for each of these models have been computed and the invariants are plotted using a "Lumley diagram" as shown in Figure 2.4 to verify their realizability.

2.2.2 **Lumley diagram** (Lumley J., 1978)

The following table shows the equations used for constructing the Lumley diagram.

Table 2.1: Lumley Diagram

Orientation States	Eigenvalues			Invariants		Remarks
	λ_1	λ_2	λ_3	II_b	III_b	
A Uniaxial alignment (ID)	1	0	0	2/3	2/9	
B Planar anisotropic (2D)	1-x	x	0	$II_b=2/9+2III_b$		$0\le x\le 1/2$
C Planar isotropic (2D Random)	1/2	1/2	0	1/6	-1/36	
D Planar axisymmetry	x	x	1-2x	$2III_b=6(II_b/6)^{1.5}$		$1/3\le x\le 1/2$
E Isotropic (3D Random)	1/3	1/3	1/3	0	0	
F Axial axisymmetry	x	x	1-2x	$2III_b=6(II_b/6)^{1.5}$		$0\le x\le 1/3$

The anisotropic tensor is defined as

$$\underline{\underline{b}} \equiv \frac{\overline{\vec{u}'\vec{u}'}}{tr\left(\overline{\vec{u}'\vec{u}'}\right)} - \frac{1}{3}\underline{\underline{\delta}} \tag{2.11}$$

where $\underline{\underline{\delta}}$ is the identity matrix. Three invariants of $\underline{\underline{b}}$ can now be defined as

$$\begin{aligned} I_b &\equiv tr\left(\underline{\underline{b}}\right) = 0 \\ II_b &\equiv tr\left(\underline{\underline{b}}\cdot\underline{\underline{b}}\right) \\ III_b &\equiv tr\left(\underline{\underline{b}}\cdot\underline{\underline{b}}\cdot\underline{\underline{b}}\right) \end{aligned} \tag{2.12}$$

Two nontrivial invariants II_b and III_b are used to describe the realizability of the tensor, which is shown in Figure 2.4 in the enclosed region.

Let $\lambda_1,\lambda_2,\lambda_3$ are the three eigenvalues of the tensor $\frac{\overline{\vec{u}'\vec{u}'}}{tr\left(\overline{\vec{u}'\vec{u}'}\right)}$. The eigenvalues $\lambda_1,\lambda_2,\lambda_3$ are independent of the choice of the coordinate system. The invariants II_b and III_b can be expressed as eigenvalues of the matrix $\underline{\underline{b}}$ as

$$II_b = (\lambda_1 - 1/3)^2 + (\lambda_2 - 1/3)^2 + (\lambda_3 - 1/3)^2 \tag{2.13}$$

$$III_b = (\lambda_1 - 1/3)^3 + (\lambda_2 - 1/3)^3 + (\lambda_3 - 1/3)^3 \tag{2.14}$$

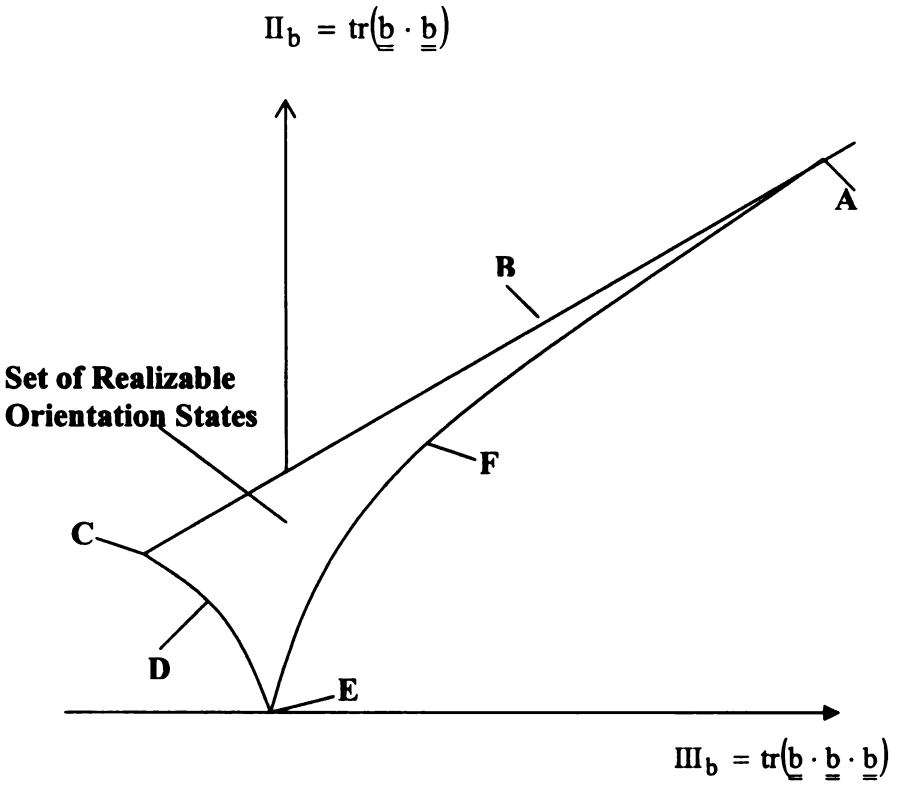

Figure 2.4: Sketch of the boundaries of the realizable states for $\underline{\underline{b}}$

As the sum of the three eigenvalues is unity, λ_3 is chosen to be dependent on λ_1 and λ_2.

A two-dimensional solution space can be obtained from equations 2.13 and 2.14.

2.2.3 Various viscous models and their approximations

The following are the various turbulence models used in Fluent 6.2

The Spalart-Allmaras Model

It is a single transport equation model proposed by Spalart et al. (1992). It treats that the production and destruction turbulent terms cancels each other and hence solves directly for a modified turbulent viscosity $\bar{\nu}$ as

$$\frac{D\bar{\nu}}{Dt} = G_\nu + \frac{1}{\sigma_\nu}\left[\frac{\partial}{\partial xj}\left\{\left(\mu + \rho\bar{\nu}\right)\frac{\partial\bar{\nu}}{\partial x_j}\right\} + C_{b2}\rho\left(\frac{\partial\bar{\nu}}{\partial x_j}\right)^2\right] - Y_\nu \qquad (2.15)$$

where Eddy – Viscosity is obtained as

$$\mu_t = \rho \bar{\nu} f_{\nu 1} , \qquad f_{\nu 1} \equiv \frac{\left(\frac{\bar{\nu}}{\nu}\right)^3}{\left(\frac{\bar{\nu}}{\nu}\right)^3 + C_{\nu 1}^3} \tag{2.16}$$

G_ν, Y_ν are the production and destruction of turbulent viscosity, ν is the molecular kinematic viscosity and $\sigma_\nu = \frac{2}{3}$, $C_{\nu 1} = 7.1$ and $C_{b2} = 0.622$.

Standard $k-\omega$ Model

The standard $k-\omega$ model in **FLUENT** is based on the Wilcox $k-\omega$ model proposed by Wilcox (1998). It belongs to the general 2-equation Eddy Viscosity Model family.

The exact transport equations for k and ε are

$$\frac{Dk}{Dt} = \frac{\partial}{\partial x_l}\left(\overline{-u_l\left(k' + \frac{p}{\rho}\right)} + \nu \frac{\partial}{\partial x_l}\right) - \overline{u_i u_l}\frac{\partial u_i}{\partial x_l} - \varepsilon \tag{2.17}$$

$$\frac{D\varepsilon}{Dt} = \frac{\partial}{\partial x_l}\left(-\overline{\varepsilon' u_l'} - \frac{2\nu}{\rho}\overline{\frac{\partial u_l'}{\partial x_j}\frac{\partial p}{\partial x_j}} + \nu\frac{\partial \varepsilon}{\partial x_l}\right) - 2\nu\frac{\partial u_i}{\partial x_j}\left(\overline{\frac{\partial u_l'}{\partial x_i}\frac{\partial u_l'}{\partial x_j}} + \overline{\frac{\partial u_i'}{\partial x_l}\frac{\partial u_j'}{\partial x_l}}\right)$$

$$- 2\nu\overline{u_l'\frac{\partial u_i'}{\partial x_j}\frac{\partial^2 u_i'}{\partial x_l \partial x_j}} - 2\nu\overline{\frac{\partial u_i'}{\partial x_j}\frac{\partial u_i'}{\partial x_l}\frac{\partial u_j'}{\partial x_l}} - 2\overline{\left(\nu\frac{\partial^2 u_i'}{\partial x_l \partial x_j}\right)^2} \tag{2.18}$$

The modeled transport equations for the turbulence kinetic energy k and the specific dissipation rate ω in the Standard $k-\omega$ model are

$$\rho\frac{Dk}{Dt} = \tau_{ij}\frac{\partial U_i}{\partial x_j} - \rho\beta^* f_{\beta^*} k\omega + \frac{\partial}{\partial x_j}\left[\left(\mu + \frac{\mu_t}{\sigma_k}\right)\frac{\partial k}{\partial x_j}\right] \tag{2.19}$$

$$\rho\frac{D\omega}{Dt}=\alpha\frac{\omega}{k}\tau_{ij}\frac{\partial U_i}{\partial x_j}-\rho\beta f_\beta\omega^2+\frac{\partial}{\partial x_j}\left[\left(\mu+\frac{\mu_t}{\sigma_\omega}\right)\frac{\partial\omega}{\partial x_j}\right] \tag{2.20}$$

where $\omega\approx\frac{\varepsilon}{k}\propto\frac{1}{\tau}$ and $\mu_t=\alpha^*\rho\frac{k}{\omega}$

Realizable k - ε Model

The term "realizable" means that the model satisfies certain mathematical constraints on the Reynolds stresses, consistent with the physics of turbulent flows. The realizable k - ε model proposed by Shih et al. (1995) address the following:

1. A new eddy-viscosity formula involving a variable C_μ originally proposed by Reynolds.
2. A new model equation for dissipation ε based on the dynamic equation of the mean-square vorticity fluctuation.

Transport Equations for the Realizable k - ε Model

The modeled transport equations for k and ε in the realizable k - ε model are

$$\frac{\partial}{\partial t}(\rho k)+\frac{\partial}{\partial x_j}(\rho k u_j)=\frac{\partial}{\partial x_j}\left[\left(\mu+\frac{\mu_t}{\sigma_k}\right)\frac{\partial k}{\partial x_j}\right]+G_k+G_b-\rho\varepsilon-Y_M \tag{2.21}$$

$$\frac{\partial}{\partial t}(\rho\varepsilon)+\frac{\partial}{\partial x_j}(\rho\varepsilon u_j)=\frac{\partial}{\partial x_j}\left[\left(\mu+\frac{\mu_t}{\sigma_\varepsilon}\right)\frac{\partial\varepsilon}{\partial x_j}\right]+\rho C_1 S\varepsilon-\rho C_2\frac{\varepsilon^2}{k+\sqrt{\nu\varepsilon}}+C_{1\varepsilon}\frac{\varepsilon}{k}C_{3\varepsilon}G_b \tag{2.22}$$

where $\mu_t=\rho C_\mu\frac{k^2}{\varepsilon}$, $C_1=\max\left[0.43,\frac{\eta}{\eta+5}\right]$, $\eta=S\frac{k}{\varepsilon}$, $S=\sqrt{2S_{ij}S_{ij}}$

In these equations, G_k represents the generation of turbulence kinetic energy due to the mean velocity gradients. G_b is the generation of turbulence kinetic energy due to

buoyancy. Y_M represents the contribution of the fluctuating dilatation in compressible turbulence to the overall dissipation rate. C_2=1.9 and $C_{1\varepsilon}$=1.44. σ_k=1.0 and σ_ε=1.2. where the ranges are C_2:1.8-2; $C_{1\varepsilon}$:1-1.8; σ_k:0.9-2; σ_ε:0.95-3 (Ching and Jaw, 1998).

Reynolds Stress Model

The Reynolds stress model proposed by Gibson et al. 91978); Launder, (1989); Launder et al. (1975) attempts to address the deficiencies of the eddy viscosity model but it is computationally more expensive.

The Reynolds Stress Transport Equations

The exact transport equations for the transport of the Reynolds stresses $\rho\,\overline{u_i'u_j'}$ may be written as follows

$$\underbrace{\frac{\partial}{\partial t}\left(\rho\overline{\vec{u}_i'\vec{u}_j'}\right)}_{\text{Local Time Derivative}} + \underbrace{\frac{\partial}{\partial x_k}\left(\rho U_k\overline{\vec{u}_i'\vec{u}_j'}\right)}_{C_{ij}\equiv\text{Convection}} = \underbrace{-\frac{\partial}{\partial x_k}\left[\rho\overline{\vec{u}_i'\vec{u}_j'\vec{u}_k'} + \overline{p\left(\delta_{kj}\vec{u}_i' + \delta_{ik}\vec{u}_j'\right)}\right]}_{D_{T,ij}\equiv\text{Turbulent Diffusion}}$$

$$\underbrace{\frac{\partial}{\partial x_k}\left[\mu\frac{\partial}{\partial x_k}\left(\overline{\vec{u}_i'\vec{u}_j'}\right)\right]}_{D_{L,ij}\equiv\text{Molecular Diffusion}} \underbrace{-\rho\left(\overline{\vec{u}_u'\vec{u}_j'}\frac{\partial\vec{u}_j'}{\partial x_k} + \overline{\vec{u}_j'\vec{u}_k'}\frac{\partial\vec{u}_i}{\partial x_k}\right)}_{P_{ij}\equiv\text{Stress Production}} \underbrace{-\rho\beta\left(g_i\overline{\vec{u}_j'\theta} + g_j\overline{\vec{u}_i'\theta}\right)}_{G_{ij}\equiv\text{Buoyancy Production}}$$

$$+ \underbrace{\overline{p\left(\frac{\partial\vec{u}_i'}{\partial x_j} + \frac{\partial\vec{u}_j'}{\partial x_i}\right)}}_{\phi_{ij}\equiv\text{Pressure Strain}} \underbrace{- 2\mu\overline{\frac{\partial\vec{u}_i'}{\partial x_k}\frac{\partial\vec{u}_j'}{\partial x_k}}}_{\varepsilon_{ij}\equiv\text{Dissipation}} \underbrace{- 2\rho\Omega_k\left(\overline{\vec{u}_j'\vec{u}_m'}\varepsilon_{ikm} + \overline{\vec{u}_i'\vec{u}_m'}\varepsilon_{jkm}\right)}_{F_{ij}\equiv\text{Production by System Rotation}} \tag{2.23}$$

2.2.4 Numerical results and verification

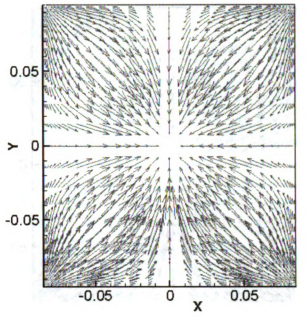

Figure 2.5: Velocity vectors for the Spalart-Allmaras model at Z/H=-0.5.

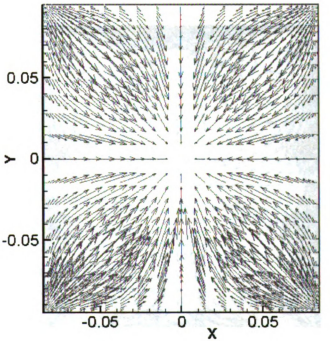

Figure 2.6: Velocity vectors for the Standard $k-\omega$ model at Z/H=-0.5.

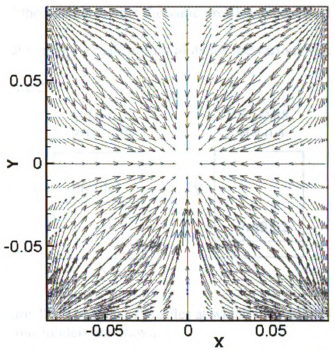

Figure 2.7: Velocity vectors for the Realizable k - ε model at Z/H=-0.5.

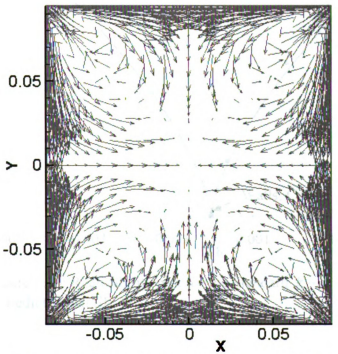

Figure 2.8: Velocity vectors for the Reynolds Stress Model at Z/H=-0.5.

Figures 2.5 to 2.8 shows the velocity vectors for various turbulent viscous models and it shows that all the models predict the same profiles except the Reynolds Stress Model. The profiles at which the realizability plots for the various viscous models are plotted are shown in Figure 2.9.

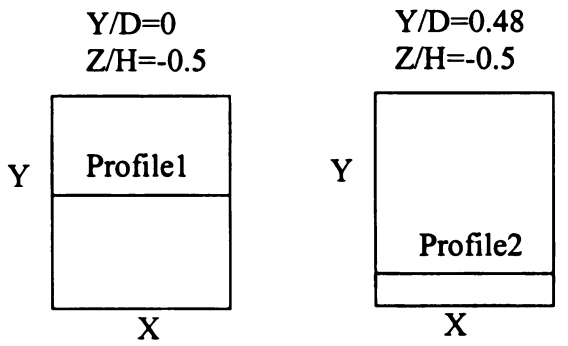

Figure 2.9: Location of profiles at which the realizability plots for the various viscous models are drawn.

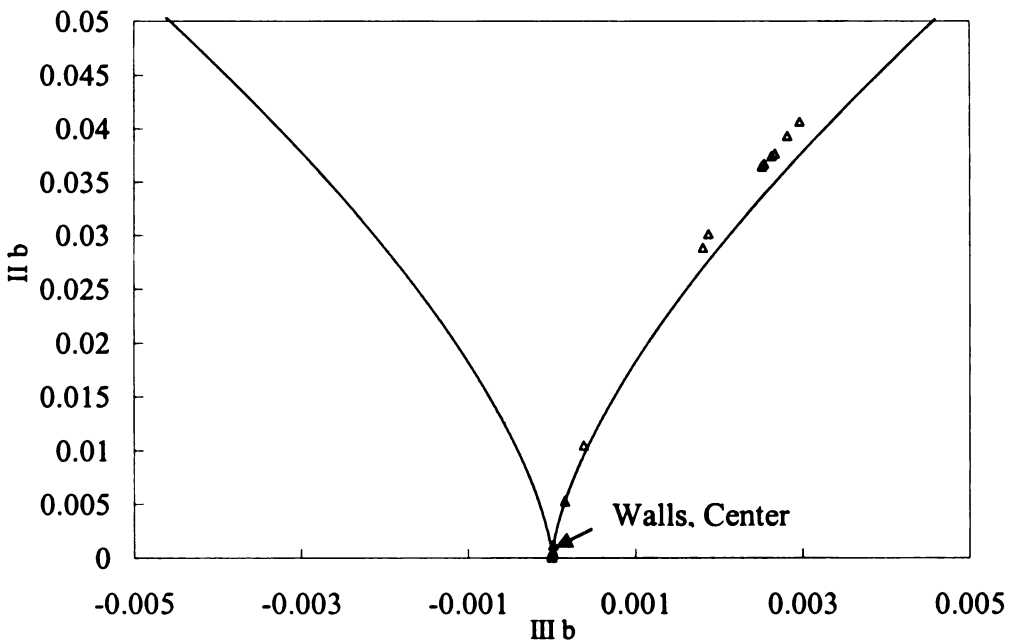

Figure 2.10: Realizability plot for the Standard $k-\omega$ model at profile1. It predicted that $III_b \approx 0$.

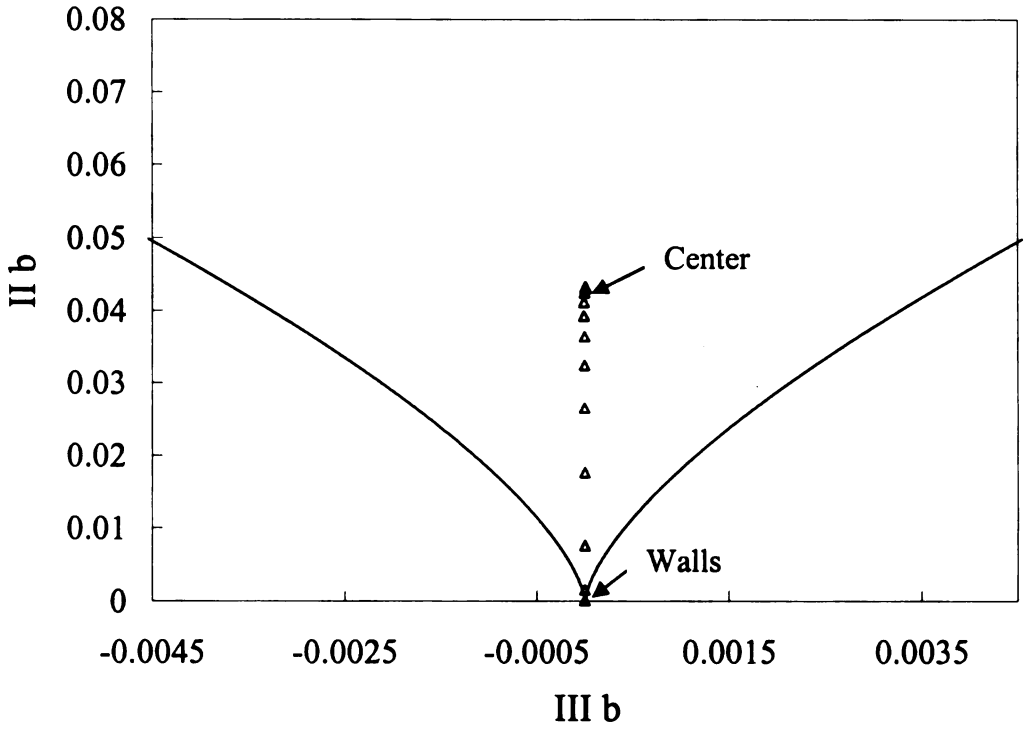

Figure 2.11: Realizability plot for the Standard $k-\omega$ model at profile 2. It predicted that $III_b \approx 0$.

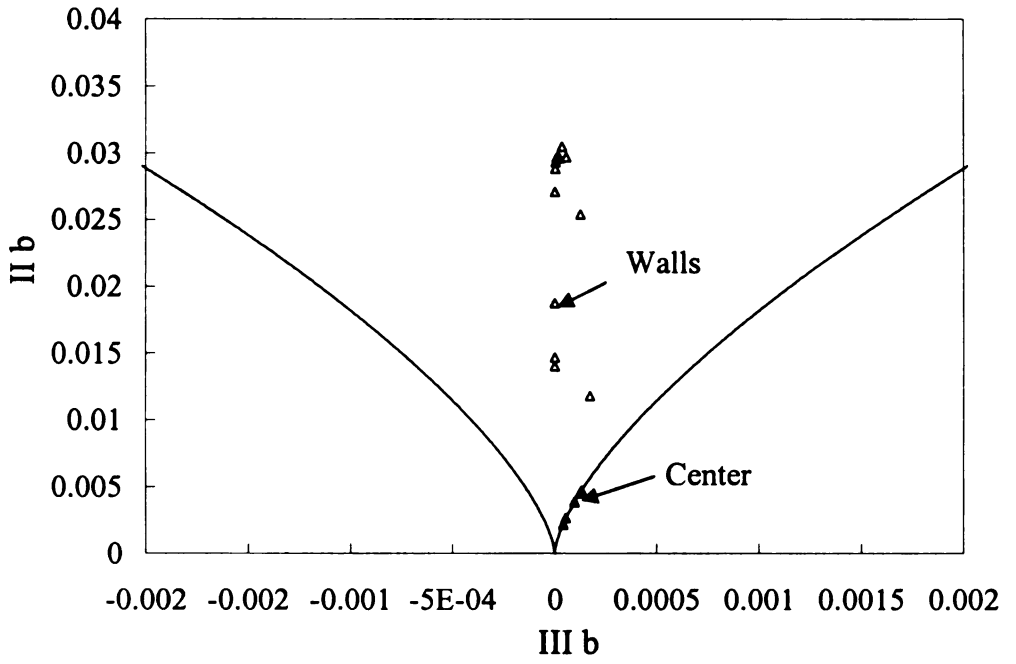

Figure 2.12: Realizability plot for the Realizable $k-\varepsilon$ model at profile 1 It predicted that $III_b \approx 0$.

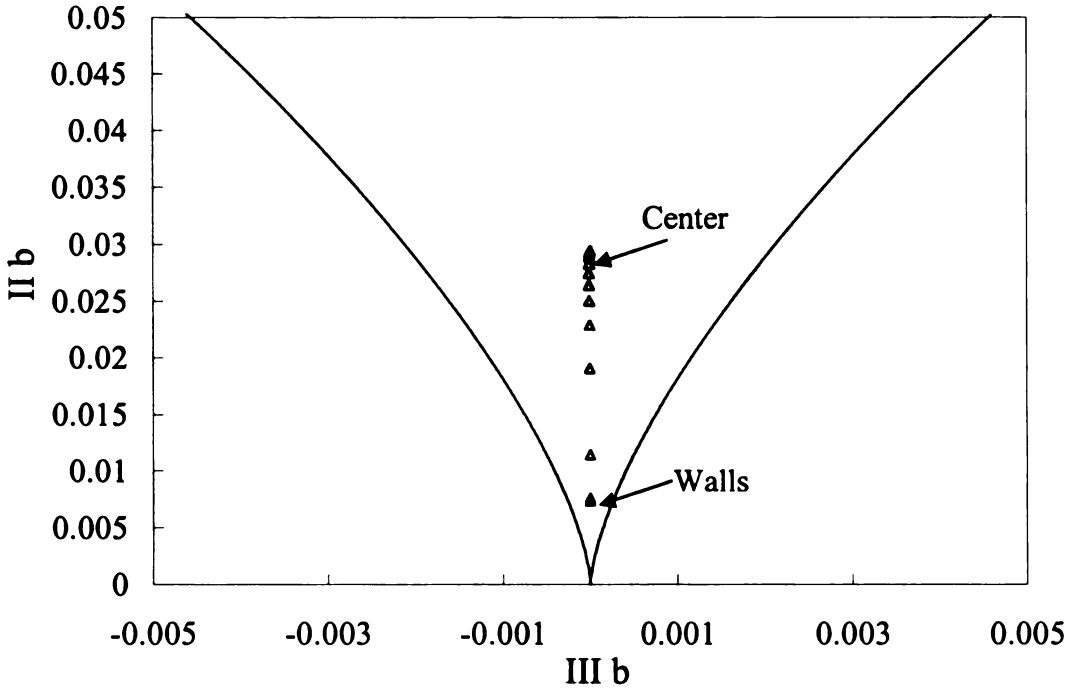

Figure 2.13: Realizability plot for the Realizable k - ε model at profile 2. It predicted that $III_b \approx 0$.

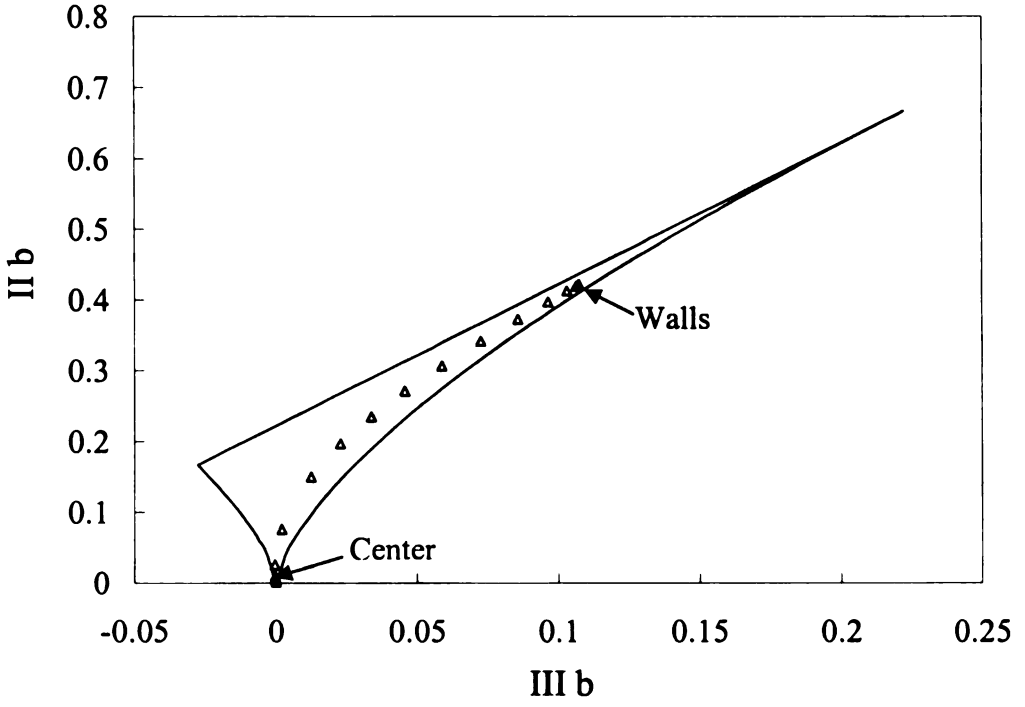

Figure 2.14: Realizability plot for the Reynolds stress model at profile 1

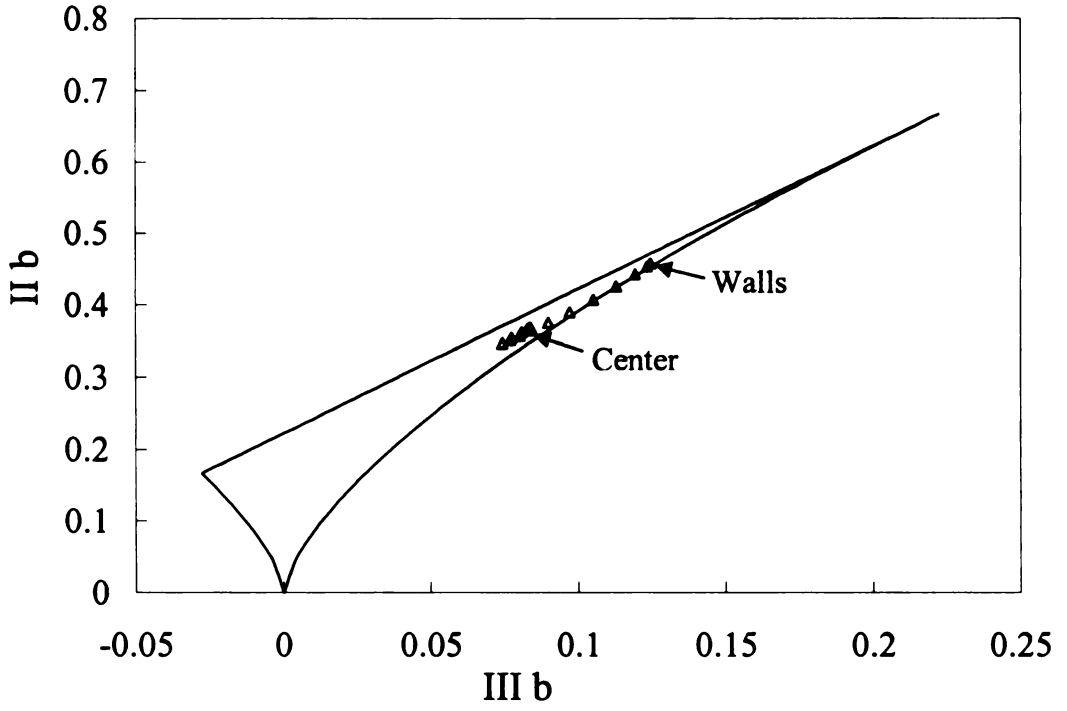

Figure 2.15: Realizability plot for the Reynolds stress model at profile 2

Figure 2.10 to 2.15 shows the realizability plots for the Standard $k-\omega$ model, the Realizable k -ε model and the Reynolds stress model. It was found that all the viscous models proved to be realizable except the Spalart-Allmaras. The Spalart-Allmaras is found to be highly unrealizable and the computed eigenvalues and invariants for this model can be found in Table C1 and C2 of Appendix C.

Also it can be seen from Figures 2.10 to 2.13 that the Standard $k-\omega$ model and Realizable k -ε model which uses the Boussinesq hypothesis predicts that the III invariant of the anisotropic tensor $\underline{\underline{b}}$ is almost zero which can be explained as follows

For a fully developed steady flow,

$$\vec{u} = u_z(x,y)\vec{e}_z \tag{2.24}$$

$$\nabla u_z = \frac{\partial u_z}{\partial x}\vec{e}_x\vec{e}_z + \frac{\partial u_z}{\partial y}\vec{e}_y\vec{e}_z \tag{2.25}$$

Since $\underline{\underline{S}} = \frac{1}{2}\left(\nabla\vec{u} + \nabla\vec{u}^{T}\right)$ (2.26)

$$\underline{\underline{S}} = \frac{1}{2}\left[\frac{\partial\vec{u}_z}{\partial x}\vec{e}_x\vec{e}_z + \frac{\partial u_z}{\partial y}\vec{e}_y\vec{e}_z + \frac{\partial\vec{u}_z}{\partial x}\vec{e}_z\vec{e}_x + \frac{\partial\vec{u}_z}{\partial y}\vec{e}_z\vec{e}_y\right] \tag{2.27}$$

$$\underline{\underline{S}} = \frac{1}{2}\begin{pmatrix} 0 & 0 & \frac{\partial\vec{u}_z}{\partial x} \\ 0 & 0 & \frac{\partial\vec{u}_z}{\partial y} \\ \frac{\partial\vec{u}_z}{\partial x} & \frac{\partial\vec{u}_z}{\partial y} & 0 \end{pmatrix} \quad \text{or} \quad \underline{\underline{S}} = \frac{1}{2}\begin{pmatrix} 0 & 0 & a \\ 0 & 0 & b \\ a & b & 0 \end{pmatrix} \tag{2.28}$$

Also since $-\rho\overline{\vec{u}'\vec{u}'} = 2\mu_t\underline{\underline{S}} - \frac{2}{3}\rho k\underline{\underline{I}}$ (2.29)

which gives $\frac{-\rho\overline{\vec{u}'\vec{u}'}}{-2\rho k} = \frac{1}{3}\underline{\underline{I}} - \frac{2\mu_t}{2\rho k}\underline{\underline{S}} = \frac{1}{3}\underline{\underline{I}} + \underline{\underline{b}}$ (2.30)

hence $\underline{\underline{b}}$ is related to $\underline{\underline{S}}$ as $\underline{\underline{b}} = \frac{-\mu_t}{\rho k}\underline{\underline{S}}$ (2.31)

The eigenvalues of the symmetric matrix $\underline{\underline{S}}$ are $\left\{0,\ \sqrt{a^2+b^2},\ -\sqrt{a^2+b^2}\right\}$

Therefore, the eigenvalues of $\underline{\underline{b}}$ are $\left\{0,\ \frac{-\mu_t}{\rho k}\sqrt{a^2+b^2},\ \frac{\mu_t}{\rho k}\sqrt{a^2+b^2}\right\}$

which results in $I_b = 0$; $II_b = 2\left(\frac{\mu_t}{\rho k}\right)^2\left(a^2+b^2\right)$ and $III_b = 0$.

Since in the simulations, the flow is not fully developed, the III_b is predicted as nearly zero as seen in Figures 2.10 to 2.13 whereas the Reynolds Stress Model does not make the above assumption and use a different model for $-\rho\,\overline{u_i'u_j'}$.

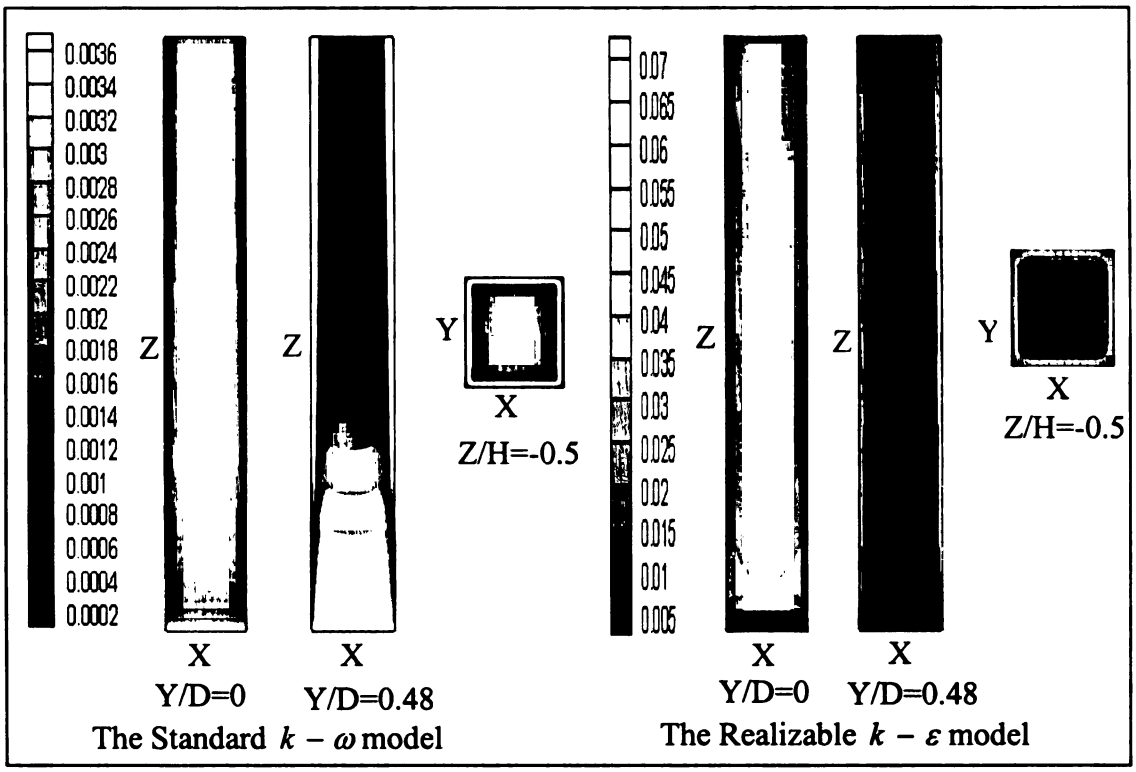

Figure 2.16: Contours of the turbulent kinetic energy for the Standard $k-\omega$ model and the Realizable $k-\varepsilon$ model at planes Y/D=0, Y/D=0.48 and Z/H=-0.5.

Figure 2.16 predicts a variation in the turbulent kinetic energy for the Standard $k-\omega$ model and the Realizable $k-\varepsilon$ model at various cross-sections in the riser.

CHAPTER 3

TURBULENT TWO PHASE FLOWS

Overview of two phase flows

Significant efforts have been made to describe the flow phenomena and dynamic behavior of the two-phase flows where the transfer of momentum, mass, and energy across the phase interface is of crucial importance.

Also, numerical simulations should satisfy strong demands in relation to approximation, especially near a wall, stability, keeping some important integral properties of governing equations and others. The Boussinesq's hypothesis between stress tensor and strain velocity tensor forms a rather simple model which enables to conduct numerical calculation up to bounded walls including a laminar sub layer. The succeeding chapters deal with the numerical simulation of turbulent bubbly flow and gas-solid flows.

3.1 COMPARISON OF DRAG INTERPHASE MODELS IN A BUBBLY FLOW

Bubbly flows play a significant role in a wide range of geophysical and industrial processes like oil transportation, mixing in chemical reactors, and elaboration of alloys, cooling of nuclear reactors, two-phase heat exchangers, aeration processes, ship hydrodynamics, and atmosphere-ocean exchanges. In a two-phase bubbly flow, the mass, momentum and energy transfer processes involved are inherently complicated and closely linked to phase distribution profiles through the strong interaction at the gas–liquid interface. Numerical simulations can help to predict two-phase dispersed flows but the capabilities of these codes are, to a large extent, limited by the closure models used to represent the momentum exchange between the dispersed and the continuous phase.

Owing to the very weak relative density of bubbles compared to that of the liquid, almost all the inertia is contained in the liquid, making inertia induced hydrodynamic forces particularly important in the prediction of bubble motion. Hence, in this section, predictions of various drag interaction models have been compared for a bubbly flow problem.

3.1.1 Case study Problem

The scope of this section is to perform steady state numerical simulations of bubbly flow in a channel using an Eulerian approach in order to compare and validate the various drag interphase models used in Fluent 6.2 namely the Schiller and Naumann model (Schiller, 1935), the Morsi and Alexander model (Morsi et al., 1972) and the symmetric model. Two Newtonian fluids, air dispersed in water is assumed with a uniform velocity of 0.3m/s and a 10 vol. % dispersed (air) phase. The air particles were assumed to be spherical with a diameter of 1mm. The simulations were performed using a realizable eddy viscosity model. The near wall treatment specification for this case can be found in Appendix A.

3.1.2 Governing equations applied to gas-liquid simulations

The governing equations used in these simulations are based on a separate treatment for each phase and are given below

The volume fraction of each phase is calculated from a continuity equation as

$$\frac{1}{\rho_{rq}}\left(\frac{\partial}{\partial t}\left(\alpha_q \rho_q\right) + \nabla \cdot \left(\alpha_q \rho_q \vec{u}_q\right)\right) = 0 \tag{3.1}$$

Where $\vec{u}_q$ is the velocity of the primary phase q and ρ_{rq} is the phase reference density of the phase q in the solution domain. The volume of phase q, is defined by

$$V_q = \int_V \alpha_q dV \tag{3.2}$$

$$\text{where } \sum_{q=1}^{n} \alpha_q = 1 \tag{3.3}$$

$$\text{The effective density of phase } q \text{ is } \hat{\rho}_q = \alpha_q \rho_q \tag{3.4}$$

Equations (3.2) and (3.3) calculate the primary-phase volume fraction.

The conservation of momentum for a fluid phase q is

$$\frac{\partial}{\partial t}\left(\alpha_q \rho_q \vec{u}_q\right) + \nabla \cdot \left(\alpha_q \rho_q \vec{u}_q \vec{u}_q\right) = -\alpha_q \nabla p + \nabla \cdot \overline{\overline{\tau}}_q + \alpha_q \rho_q \vec{g} + \sum_{p=1}^{n} \left(K_{pq}\left(\vec{u}_p - \vec{u}_q\right)\right) \tag{3.5}$$

Here $\vec{g}$ is the acceleration due to gravity and P is the pressure shared by all phases.

$$\overline{\overline{\tau}}_q = \alpha_q \mu_q \left(\nabla \vec{u}_q + \nabla \vec{u}_q^T\right) + \alpha_q \left(\lambda_q - \frac{2}{3}\mu_q\right) \nabla \cdot \vec{u}_q \overline{\overline{I}} \tag{3.6}$$

Here μ_q and λ_q are the shear and bulk viscosity of phase q.

3.1.3 Theoretical formulation of various drag interphase models

Momentum exchange between the phases is based on the value of the fluid-fluid exchange coefficient K_{pq}. It is the drag function that differs among the exchange-coefficient models. The following are the three different drag interphase momentum theories found in FLUENT for the gas-liquid flow.

The exchange coefficient can be written in the following general form as

$$K_{pq} = \frac{\alpha_q \alpha_p \rho_p f}{\tau_p} \tag{3.7}$$

where q is the primary phase and p is the secondary phase. The particle relaxation time is given as

$$\tau_p = \frac{\rho_p d_p^2}{18\mu_q} \tag{3.8}$$

where drag function,

$$f = \frac{C_D \,\mathrm{Re}}{24} \tag{3.9}$$

and d_p is the particle diameter

The drag coefficient given by various models is as follows

The Schiller-Naumann Model (Schiller, 1935)

$$C_D = \begin{cases} 24\left(1 + 0.15\,\mathrm{Re}^{0.687}\right)/\mathrm{Re} & \mathrm{Re} \le 1000 \\ 0.44 & \mathrm{Re} > 1000 \end{cases} \tag{3.10}$$

The Morsi and Alexander Model (Morsi et al., 1972)

$$C_D = a_1 + \frac{a_2}{\mathrm{Re}} + \frac{a_3}{\mathrm{Re}^2} \tag{3.11}$$

$$a_1, a_2, a_3 = \begin{cases} 0,24,0 & 0 < \mathrm{Re} < 0.1 \\ 3.690,22.73,0.0903 & 0.1 < \mathrm{Re} < 1 \\ 1.222,29.1667,-3.8889 & 1 < \mathrm{Re} < 10 \\ 0.61617,46.50,-116.67 & 10 < \mathrm{Re} < 100 \\ 0.3644,98.33,-2778 & 100 < \mathrm{Re} < 1000 \\ 0.357,148.62,-47500 & 1000 < \mathrm{Re} < 5000 \\ 0.46,-490.546,578700 & 5000 < \mathrm{Re} < 10000 \\ 0.5191,-1662.5,5416700 & \mathrm{Re} \ge 10000 \end{cases} \tag{3.12}$$

The Symmetric Model

$$K_{pq} = \frac{\alpha_p\left(\alpha_p\rho_p + \alpha_q\rho_q\right)f}{\tau_{pq}}, \quad \tau_{pq} = \frac{\left(\alpha_p\rho_p + \alpha_q\rho_q\right)d_p^2}{18\left(\alpha_p\mu_p + \alpha_q\mu_q\right)} \tag{3.13}$$

$$f = \frac{C_D \,\mathrm{Re}}{24} \quad \text{where } C_D = \begin{cases} 24\left(1 + 0.15\,\mathrm{Re}^{0.687}\right)/\mathrm{Re} & \mathrm{Re} \le 1000 \\ 0.44 & \mathrm{Re} > 1000 \end{cases} \tag{3.14}$$

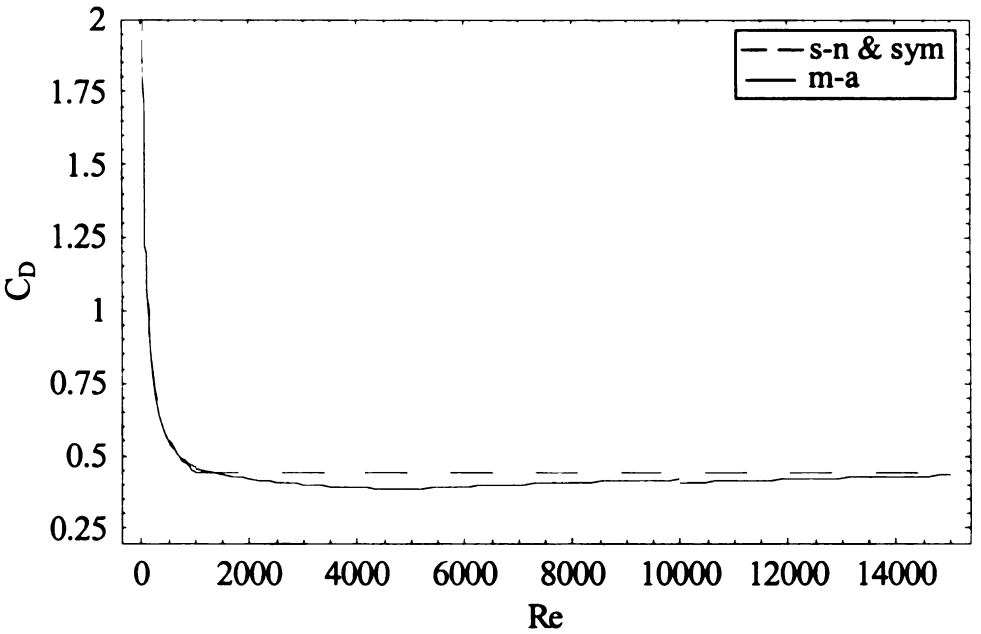

Figure 3.1: Plot of comparison of the various drag models for the bubbly flow.

3.1.4 Numerical results and discussions

In Figure 3.2, the locations at which the points extracted to produce Figures 3.3 to Figure 3.8 are shown.

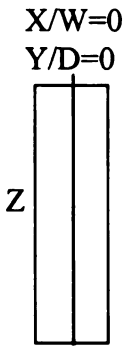

Figure 3.2: Location of profile at which the various drag models are compared.

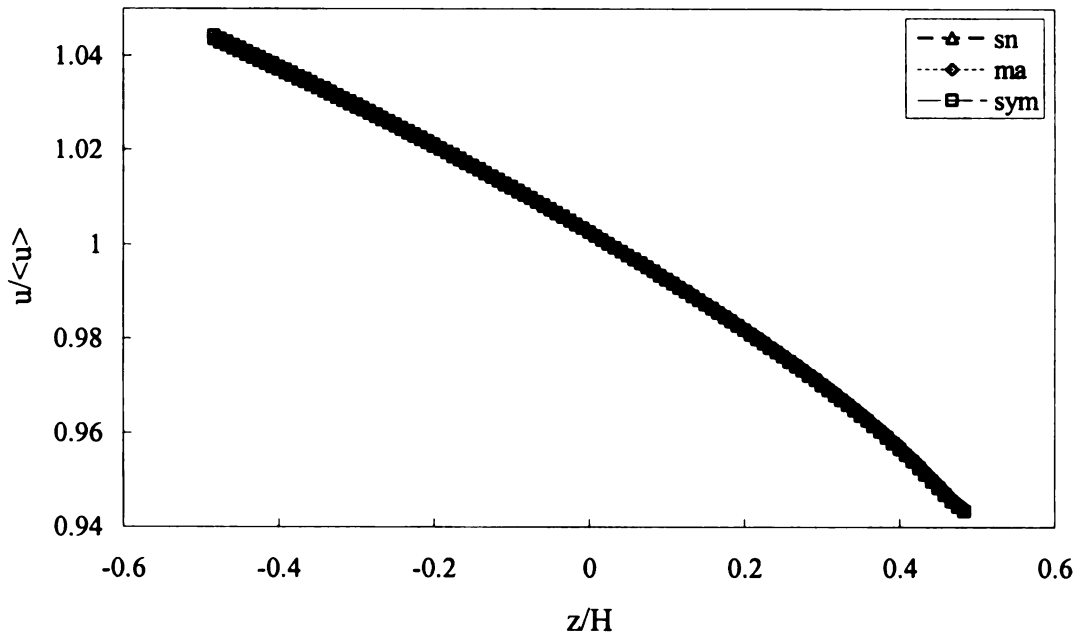

Figure 3.3: Plot of dimensionless axial velocity of water vs. dimensionless height for the Schiller-Naumann model, the Morsi and Alexander model and the Symmetric model (sn, ma, sym). All models give similar results.

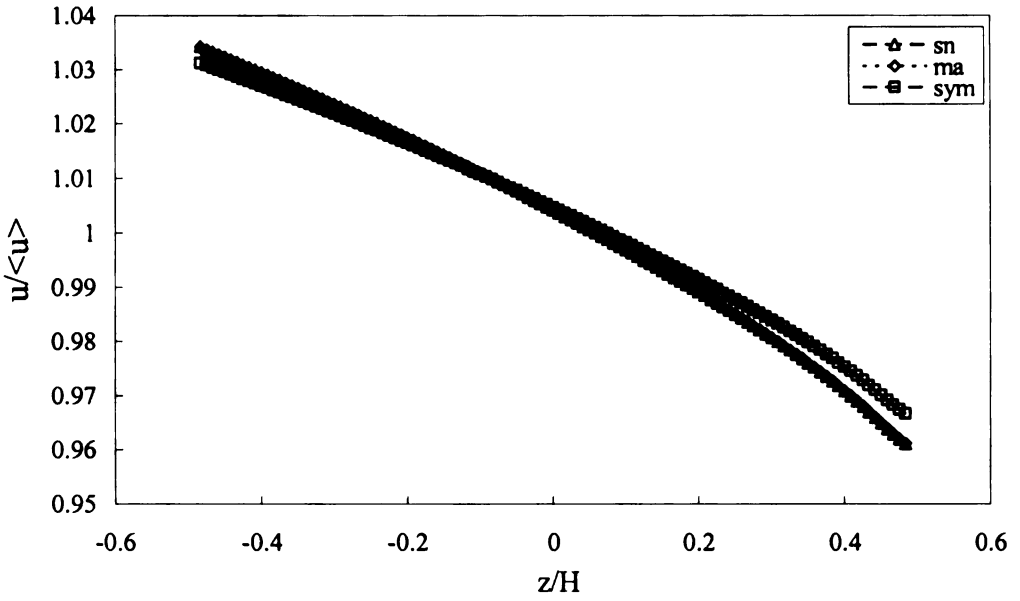

Figure 3.4: Plot of dimensionless axial velocity of air vs. dimensionless height for the Schiller-Naumann model, the Morsi and Alexander model and the Symmetric model (sn, ma, sym). All models give similar results.

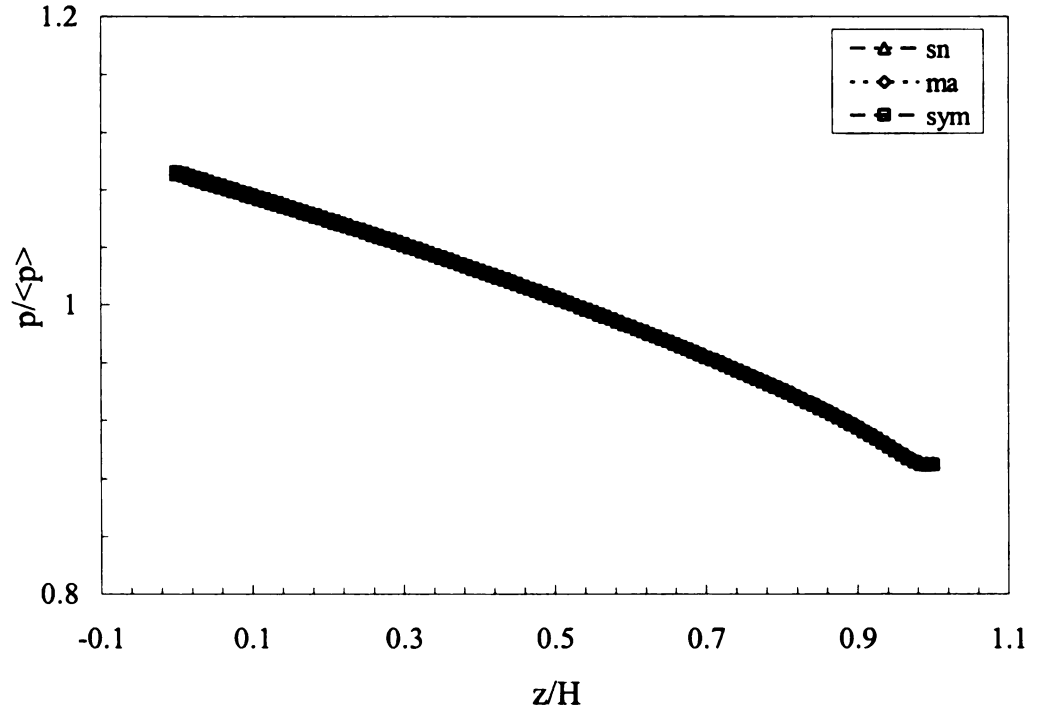

Figure 3.5: Plot of dimensionless axial dynamic pressure of water vs. dimensionless height for the Schiller-Naumann model, the Morsi and Alexander model and the Symmetric model (sn, ma, sym). All models give similar results.

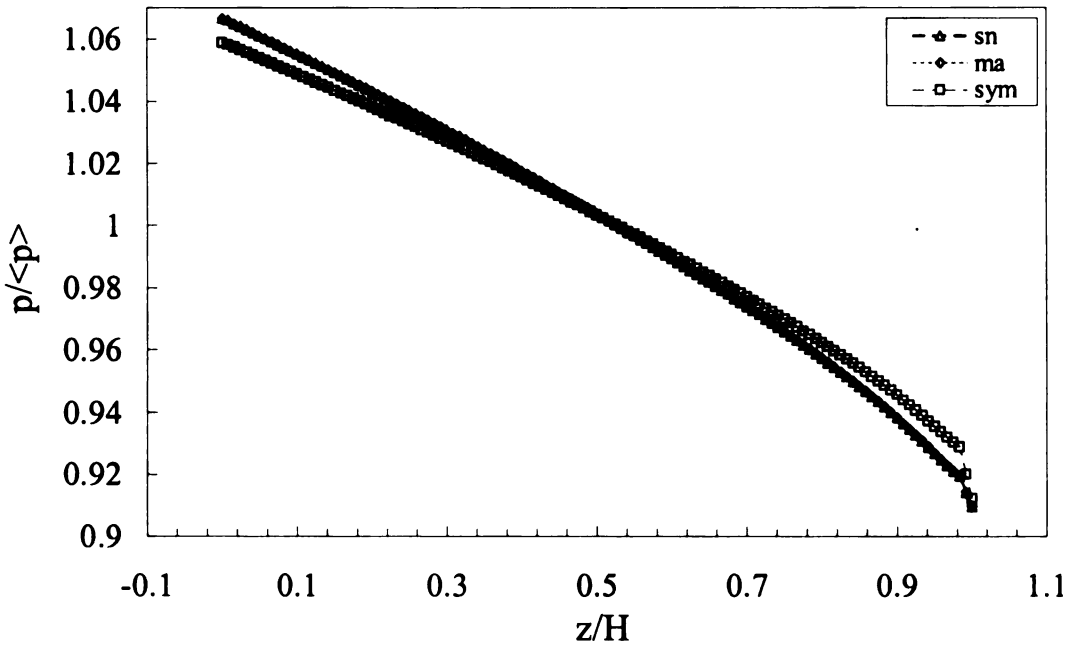

Figure 3.6: Plot of dimensionless axial dynamic pressure of air vs. dimensionless height for the Schiller-Naumann model, the Morsi and Alexander model and the Symmetric model (sn, ma, sym). All models give similar results.

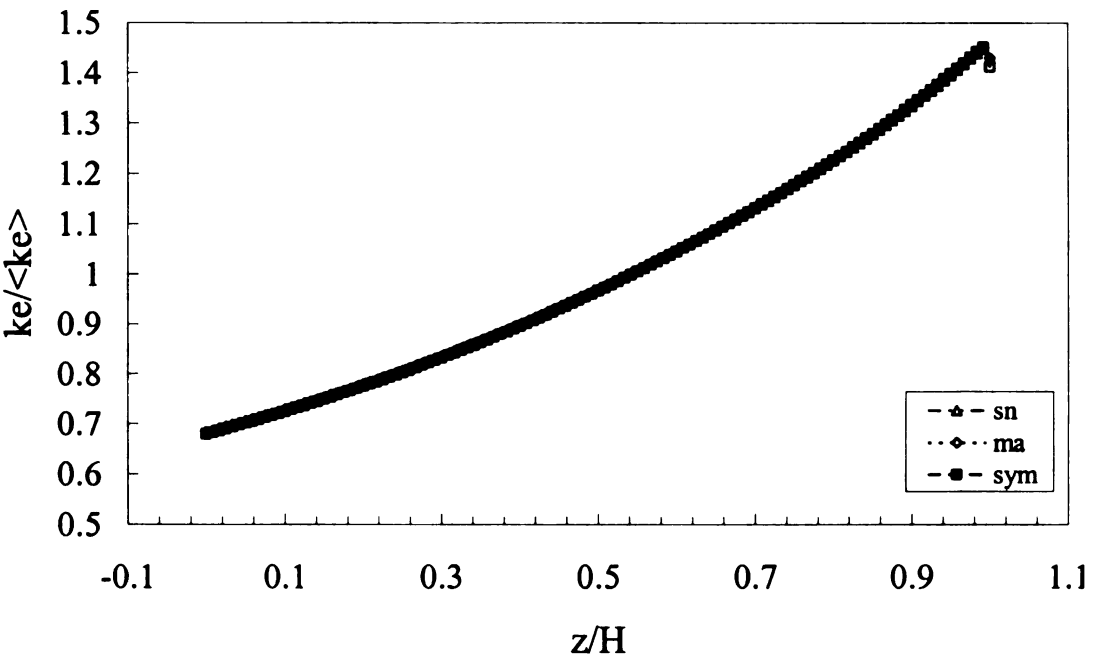

Figure 3.7: Plot of dimensionless axial turbulent kinetic energy of water vs. dimensionless height for the Schiller-Naumann model, the Morsi and Alexander model and the Symmetric model (sn, ma, sym). All models give similar results.

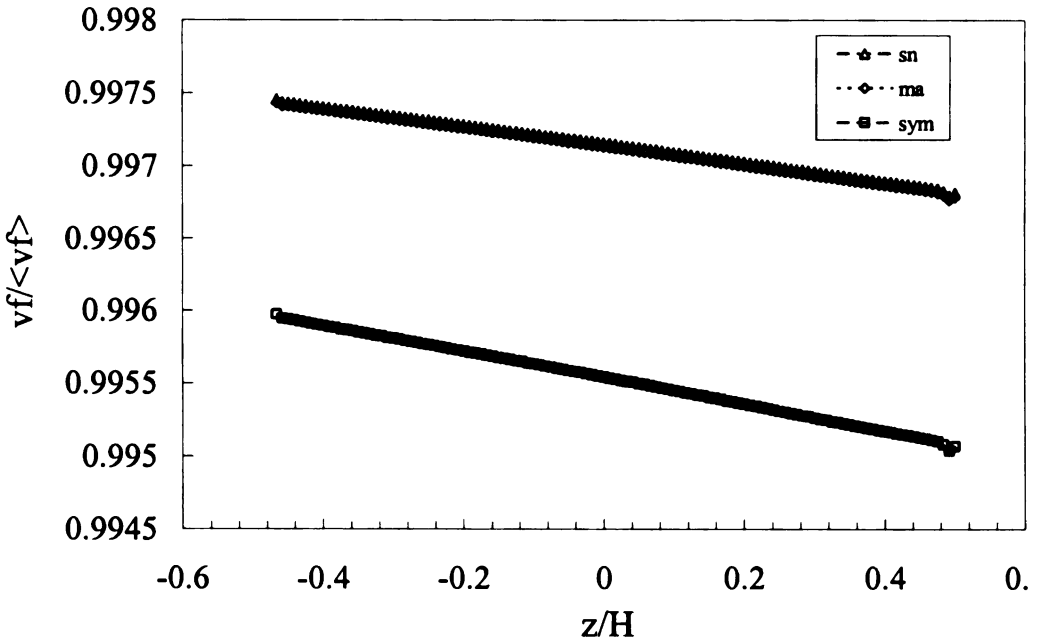

Figure 3.8: Plot of dimensionless axial volume fraction of air vs. dimensionless height for the Schiller-Naumann model, the Morsi and Alexander model and the Symmetric model (sn, ma, sym). All models give similar results with a very slight difference.

From Figures 3.2 to Figure 3.8, it can be seen that all the correlations studied predict similar values of global quantities such as the velocity, pressure, turbulent kinetic energy and concentration of the dispersed phase for the steady state solution. From the Figure 3.1 it can be seen that for the Reynolds number of 10,000 the C_D values given by the various drag interphase models is about the same.

The profiles at which the realizability plots are drawn for the secondary phase is shown in Figure 3.9.

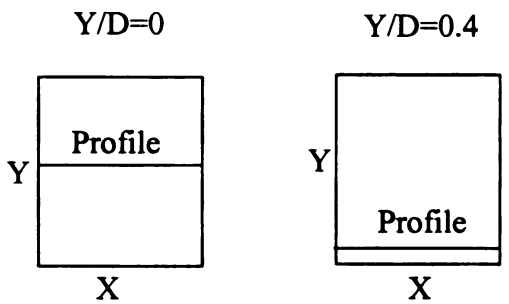

Figure 3.9: Location of profiles at which the realizability plots are drawn for Z/H = -0.5

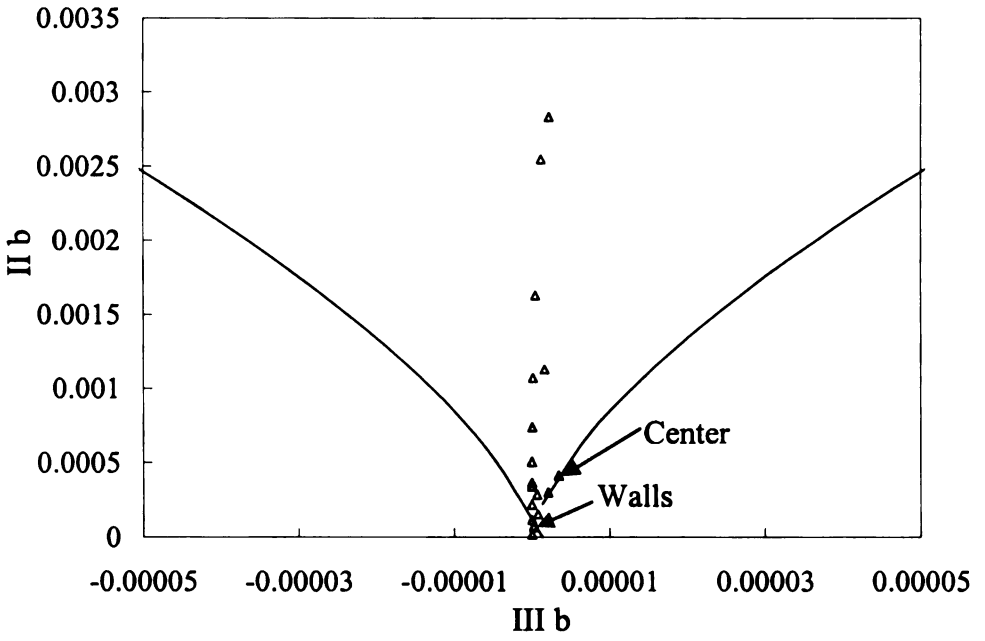

Figure 3.10: Realizability plot for the secondary phase (air) in the gas-liquid simulations at profile 1. The realizable $k-\varepsilon$ model predicted that $III_b \approx 0$.

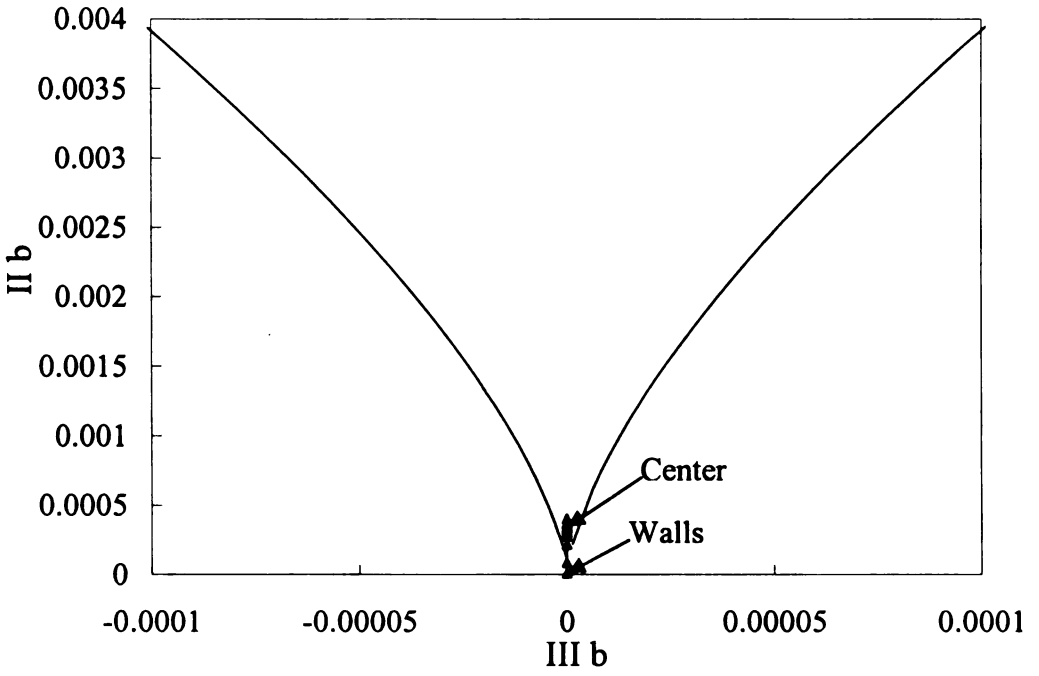

Figure 3.11: Realizability plot for the secondary phase (air) in the gas-liquid simulations at profile 2. The realizable $k-\varepsilon$ model predicted that $III_b \approx 0$.

The realizability plots for the secondary phase (air) using the Schiller-Naumann drag interphase model is as shown in Figures 3.10 and 3.11. In the two-phase simulations of gas-liquid flows, the realizable k - ε model proves to be realizable for the secondary phase (air) while it shows to be highly unrealizable for the primary phase (water) and the computed eigenvalues and invariants for this unrealizable case can be found in Table C3 and C4 of Appendix C. Again, it can be seen from the above figure that the III invariant of the anisotropic tensor $\underline{\underline{b}}$ is almost zero.

Also, all the various drag models studied in this case predicts exactly the same realizability values with a negligible difference. For the sake of brevity; the realizability plots for all the other drag models are not presented. Figure 3.12 shows a variation in the turbulent kinetic energy in the riser.

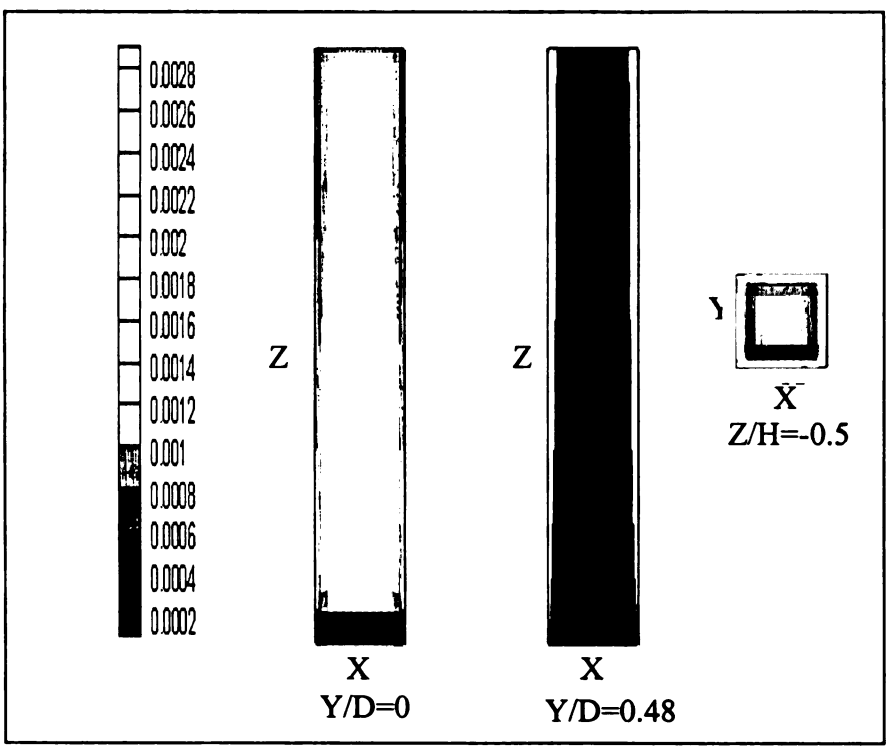

Figure 3.12: Contours of the turbulent kinetic energy for the primary phase (water) at planes Y/D=0, Y/D=0.48 and Z/H=-0.5.

3.2 NUMERICAL SIMULATION OF A GAS-SOLID FLOW IN A RISER

The scope of this section is to perform the transient numerical simulations for the gas-solid flow under isothermal conditions in a riser using a realizable eddy viscosity model. The purpose is to evaluate the ability of the multiphase model to capture important physical phenomena encountered in a catalytic riser. Further, the experimental findings of Ibsen et al. (2001) were used here for evaluating the quality of the numerical predictions.

Transient simulations of gas-solid flows in a riser have been performed using a realizable "eddy" viscosity model proposed by Shih et al. (1995) to account for the transport of mean momentum by turbulent fluctuations. The dispersed turbulence model and a granular model were used to model the gas and solid phase respectively. Air is considered as a primary phase with constant density and viscosity. The solid particles are assumed to be spherical in shape with a uniform density. The various parameters used in this simulation are shown in Table 3.1. The near wall treatment specifications can be found in Appendix A.

3.2.1 Assumptions made in the gas-solid simulations

Due to the complex nature of the flows associated with the riser, the following simplifications in the geometry and particle size were introduced for the purpose of this exploratory study.

Particle size: Since the simulations presented here were based on three dimensional modeling of the gas-solid flow, the numerical modeling was restricted to two-phase simulations with one solid phase with a representative particle diameter for the particle size distribution in the experiments in order to keep the computational time down.

Circulating Fluidized Bed Geometry: The inlet is located at the bottom and the outlet is located at the top, thereby neglecting the effects of the inlet and the exit locations, which are placed at the side on the actual riser.

3.2.2 General guidelines for mathematical modeling in fluidization

Harris et al. (1996) present a classification of models for simulating circulating fluidized beds. According to the authors there are three types of mathematical models:

1. Models that predict the axial variation of the density of solids and disregard its lateral variations.
2. Models that predict the span wise variation of the density of solids and the high average slipping velocities, accounting for two or more regions of different flow characteristics.
3. Models that apply the fundamental conservative equations of the fluid dynamics for predicting the two-phase gas-solids flow.

The first two types of models are mostly used for preliminary design, mainly for investigating the effects on the process of geometry and operational conditions. These models can easily include chemical kinetics for simulating the performance of reactors. The models of the third type, as for example a two-fluid model, are more suitable for research allowing, for instance, the behavior of flow local structures and the effects of local geometry to be studied. Figure 3.13 presents actual lines and tendencies for the third type of mathematical modeling. There are two major tendencies for modeling, following a treatment either Eulerian for both phases (Eulerian formulation) or Eulerian for the fluid phase and Lagrangian for the particulate phase (Eulerian-Lagrangian formulation).

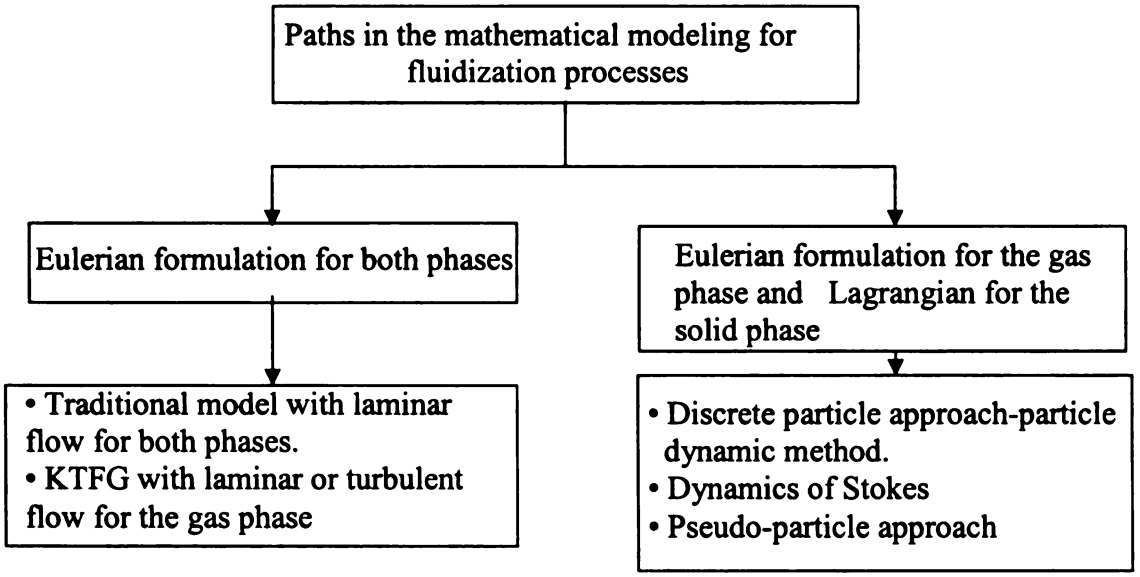

Figure 3.13: Sketch outlining the actual lines and tendencies for the third type of mathematical modeling in fluidization.

In the Eulerian formulation both phases are treated as a continuum. Each phase is modeled separately in terms of a system of conservative equations for mass, momentum and energy. The conservative equations present terms accounting for interface interaction, which are related to mass, momentum and energy exchanges through the interface. In their traditional formulation, those models require the dynamic viscosity of the solid phase to be specified. A constant value for the solids viscosity can be obtained through momentum balances applied to experimental data (Gidaspow et al., 1992).

The traditional Eulerian formulation has been extensively applied to fluidization (Gidaspow et al., 1983; Gidaspow, 1986; Bouillard et al., 1989). A new approach has been developed by a number of researchers for dealing with solids phase viscosity (Jenkins et al., 1983; Lun et al., 1984; Jenkins et al., 1985). This is the kinetic theory of granular flow, which is based on the kinetic theory of dense gases (Chapman et al., 1970).

Bagnold, (1954) and Gidaspow, (1994) is generally credited with starting the kinetic theory approach of granular flow. The kinetic theory of granular flow is based on an analogy between the flow of granular materials and the motion of gas molecules (Peirano, 1996). In spite of allowing the direct determination of the solids viscosity, the kinetic theory of granular flow implies in more complex numerical procedures and higher computation times. Gidaspow, (1994) was the first to present a detailed theoretical derivation of Kinetic Theory of Granular Flow and to consider its application to particulate flows.

In Eulerian-Lagrangian formulation only the gas phase is assumed as a continuum. This approach allows a better understanding of the particle-particle interactions. However, the Eulerian-Lagrangian formulation requires a complete set of equations (Newton's second and third laws) to be written for each particle in the flow field, difficulting its application to fluidization in view of computational limitations. Otherwise it is a very useful tool for the development of new rheological models for fluidized suspensions, and to enhance the formulation of closing laws required by two-fluids Eulerian models.

The analysis of gas-solid flows is complex because of the strong coupling between the solid and gas phases. The gas flows through the interstitial spaces or voids created by the particles, moving the particles and re-arranging the gas flow paths. The gas phase exerts a drag force on the solids; the solids exert an equal and opposite force drag on the gas. Furthermore, the pressure gradients created in the gas flow give rise to pressure forces on the particulate phase. Density differences between the two phases cause buoyancy driven flows. Thus the two phases exchange momentum and energy.

3.2.3 Governing equations applied to gas-solid simulations

The mathematical model is based on a three-dimensional Eulerian realizable $k-\varepsilon$ multiphase model. The gas phase calculations are done using a continuum approach. The conservation equations for the solid phases are based on the kinetic theory for granular flow. The governing equations for the gas solid model may be summarized as follows. The volume fraction of each phase k is calculated from a continuity equation

$$\frac{\partial}{\partial t}(\alpha_k \rho_k) + \nabla \cdot (\alpha_k \rho_k \vec{u}_k) = 0 \tag{3.15}$$

where α_k, ρ_k and $\vec{u}_k$ are the volume fraction, density and velocity of phase k respectively. The conservation of momentum for a fluid phase q is

$$\frac{\partial}{\partial t}(\alpha_q \rho_q \vec{u}_q) + \nabla \cdot (\alpha_q \rho_q \vec{u}_q \vec{u}_q) = -\alpha_q \nabla p + \nabla \cdot \overline{\overline{\tau_q}} + \alpha_q \rho_q \vec{g} + \sum_{q=1}^{n} K_{pq}(\vec{u}_p - \vec{u}_q) \tag{3.16}$$

The solid-phase stresses are derived by making an analogy between the random particle motion arising from particle-particle collisions and the thermal motion of molecules in a gas, taking into account the inelasticity of the granular phase. As is the case for a gas, the intensity of the particle velocity fluctuations determines the stresses, viscosity, and pressure of the solid phase. The kinetic energy associated with the particle velocity fluctuations is represented by a "pseudo thermal" or granular temperature which is proportional to the mean square of the random motion of particles.

The conservation of momentum for the solid phase s is given as

$$\frac{\partial}{\partial t}(\alpha_s \rho_s \vec{u}_s) + \nabla \cdot (\alpha_s \rho_s \vec{u}_s \vec{u}_s) = -\alpha_s \nabla p - \nabla p_s + \nabla \cdot \overline{\overline{\tau_s}} + \alpha_s \rho_s \vec{g} + \sum_{q=1}^{n} K_{qs}(\vec{u}_q - \vec{u}_s) \tag{3.17}$$

The stress-strain tensor is given as

$$\overline{\overline{\tau_q}} = \alpha_q \mu_q \left(\nabla \vec{u}_q + \nabla \vec{u}_q^T\right) + \alpha_q \left(\lambda_q - \frac{2}{3}\mu_q\right) \nabla \cdot \vec{u}_q \overline{\overline{I}} \tag{3.18}$$

where p and $\vec{g}$ are pressure and gravitational acceleration respectively. μ_q and λ_q is the shear and bulk viscosity of phase q; K_{sq} is the drag coefficient between the phase s and q. The solid phase pressure p_s, the bulk viscosity λ_s and the shear viscosity μ_s are derived from the kinetic theory for granular flow.

The interphase momentum transfer coefficient between gas and solid is modeled as proposed by Gidaspow, (1986) which is

$$K_{sq} = \frac{3}{4} C_D \frac{\alpha_s \alpha_q \rho_q \left|\vec{u}_s - \vec{u}_q\right|}{d_s} \alpha_q^{-2.65} \tag{3.19}$$

$$\text{where } C_D = \frac{24}{\alpha_q \operatorname{Re}_s}\left[1 + 0.15\left(\alpha_q \operatorname{Re}_s\right)^{0.687}\right] \tag{3.20}$$

3.2.4 Governing equations applied in the kinetic theory of granular flow

The following are the equations applied in the kinetic theory of granular flow

Granular Temperature

The viscosities need the specification of the granular temperature for the solids phase for which an algebraic equation proposed by Syamlal et al. (1993) is

$$0 = \left(-p_s \overline{\overline{I}} + \overline{\overline{\tau_s}}\right) : \nabla \vec{u}_s - \gamma \theta_s + \phi_{qs} \tag{3.21}$$

where $\left(-p_s \overline{\overline{I}} + \overline{\overline{\tau_s}}\right) : \nabla \vec{u}_s$ is the generation of energy by the solid stress tenor, $\gamma \theta_s$ is the collisional dissipation of energy and ϕ_{qs} is the energy exchange between the fluid or solid phase and the solid phase.

The collisional dissipation of energy $\gamma\theta_s$ represents the rate of energy dissipation within the solids phase due to collisions between particles which is given by Lun et al. (1984) as

$$\gamma\theta_s = \frac{12(1-e_{ss}^2)g_{0,ss}}{d_s\sqrt{\pi}}\rho_s\alpha_s^2\theta_s^{3/2} \tag{3.22}$$

The transfer of the kinetic energy of random fluctuations in particle velocity from the solids phase to the fluid or solid phase is represented by ϕ_{qp} and is given by Gidaspow et al. (1972).

$$\phi_{qs} = -3K_{qs}\theta_s . \tag{3.23}$$

Solids phase shear viscosity (neglecting frictional viscosity)

It is given as the sum of kinetic and collisional shear viscosities as

$$\mu_s = \underbrace{\frac{10\rho_s d_s\sqrt{\theta_s\pi}}{96\alpha_s(1+e_{ss})g_{0,ss}}\left[1+\frac{4}{5}g_{0,ss}\alpha_s(1+e_s)\right]^2}_{\mu_{s,kin}} + \underbrace{\frac{4}{5}\alpha_s\rho_s d_s g_{0,ss}(1+e_{ss})\left(\frac{\theta_s}{\pi}\right)^{1/2}}_{\mu_{s,coll}} \tag{3.24}$$

Granular Bulk Viscosity

The solids bulk viscosity accounts for the resistance of the granular particles to compression and expansion. The expression for this is given by Lun et al. (1984).

$$\lambda_s = \frac{4}{3}\alpha_s\rho_s d_s g_{0,ss}(1+e_{ss})\left(\frac{\theta_s}{\pi}\right)^{1/2} \tag{3.25}$$

For granular flows in the regime where the solids volume fraction is less than its maximum allowed value, a solids pressure is calculated independently and used for the pressure gradient term, ∇p_s, in the granular-phase momentum equation. Because a

Maxwellian velocity distribution (which has a temperature term) is used for the particles, a granular temperature is introduced into the model, and appears in the expression for the solids pressure and viscosities.

The solids pressure is composed of a kinetic term and a second term due to particle collisions and is given by Lun et.al. (1984) as

$$p_s = \alpha_s \rho_s \theta_s + 2\rho_s (1+e_{ss}) \alpha_s^2 g_{0,ss} \theta_s \tag{3.26}$$

where e_{ss} is the coefficient of restitution for particle collisions, $g_{0,ss}$ is the radial distribution function, and θ_s is the granular temperature.

Radial distribution Function

It specifies a correction factor that modifies the probability of collisions between grains when the solid granular phase becomes dense. The expression for this is given by Sinclair et al. (1989)

$$g_0 = \left[1 - \left(\frac{\alpha_s}{\alpha_{s,\max}} \right)^{\frac{1}{3}} \right]^{-1} \tag{3.27}$$

3.2.5 Experimental set up of the 1/9 scale Cold Circulating Fluidized Bed Boiler

The dimensions of the experimental set up of Ibsen et al. (2001) were 1.5 m x 0.19 m x 0.17 m corresponding to Height(x) x Depth(y) x width (z) respectively. A cyclone was located at the rear of the riser, 1.2 m above the primary air distributor to separate the solids, which passed a particle seal designed as a bubbling bed, before being reintroduced in the lower part of the riser. No secondary air was used. The amount of solids recirculated was adjusted to give a pressure drop across the riser equal to 2.7 KPa

(corresponding to 8KPa in the full-scale boiler). A detailed description of the model is provided by Johnsson et al. (1999).

3.2.6 Numerical configuration of the gas-solid simulations

The numerical flow parameters applied in the gas-solid simulations are tabulated in Table 3.1.

Table 3.1: Parameters for the gas-solid simulations

Dimensions of the geometry (H X W X D)	XxYxZ	1.2 x 0.17 x 0.19
Number of Mesh Cells	N_{cell}	146,880
Gas Density	ρ_g	1.2 kg/m3
Gas Velocity	V_g	1.0 m/s
Gas Viscosity	μ_g	1.8 E-05 kg/ms
Particle diameter	d_p	45 μ m
Particle Density	ρ_p	7800 kg/m3
Amount of Solids Used	m_s	9 kg
Volume fraction of solid	α_s	0.03572
Restitution coefficient	e	0.95
Maximum Solid Packing	e_s ,max	0.64

A uniform plug flow is assumed for the gas phase at the inlet with a superficial velocity of 1.0 m/s (Reynolds number=12,156). The inlet flux of the solid phase is assumed to be equal to the outlet flux. The simulation imposes a no-slip condition at the wall for all phases. Zero initial velocity was specified for the solid phase in the flow domain with the solids being evenly distributed in the lower half of the riser. Due to the large number of cells in three dimensions, the simulations were terminated after 20s of real time and the averaged results were obtained which was found to be adequate. A mean volume length diameter of d_p = 45 μ m. is used for the solid phase (Peirano et al., 2000). About 9 kg. of

solids were used in the simulations to give a pressure drop over the riser height which is comparable to the experiments.

3.2.7 Simulation time

Simulations of fluidized beds with about 9 kg of solids took about 8 days to simulate 20 seconds of real time. The simulations were run on 6 nodes with a 2.2 GHz processor. In comparison Zhang et al. (2001) used 101 days to simulate 21 s with their fine grid on a SGI Origin 200.

3.2.8 Numerical results and discussions

The numerical predictions are plotted against the experimental findings along profiles 1, 2, 3, 4 and 5 are shown in Figure 3.14. The H_{exp}=1.5m.

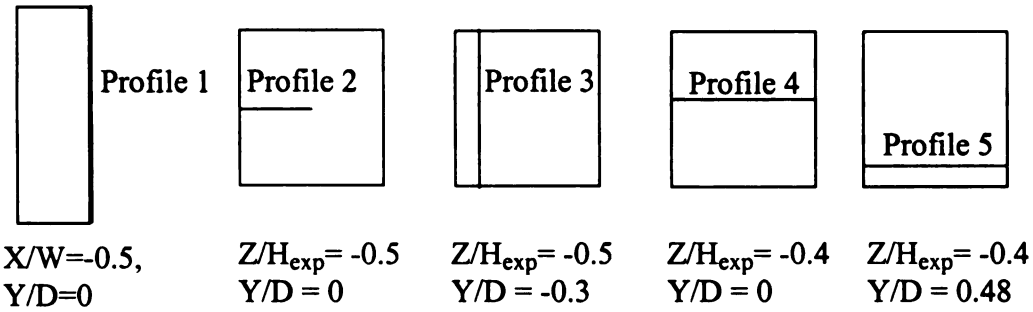

Figure 3.14: Locations of profiles used for plotting the gas-solid results

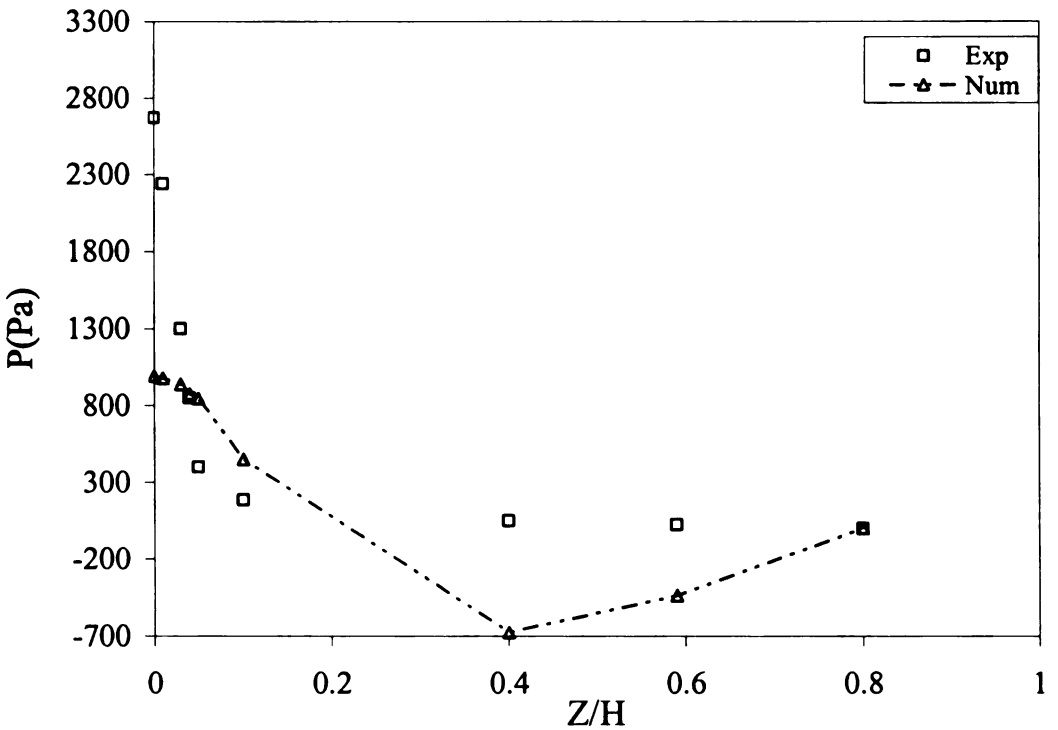

Figure 3.15: Plot of comparison between the measured (Ibsen et al., 2001) and computed static pressure vs. dimensionless height at profile 1. It can be seen that a linear pressure drop is predicted which deviates greatly from the experiments.

Static pressure

Figure 3.15 shows the computed and measured static pressure drop as a function of riser height at profile 1. The numerical results fail to predict the right order of pressure drop. The simulations showed a linear pressure drop which deviates strongly from the non-linear findings of the experiments. Also the pressure drop at the inlet is predicted as 5kPa which was only 2.7kPa in the experiments.

Particle velocities

The particle velocities at profile 2 and 3 are shown in Figures 3.16 to 3.19. It shows that the mean volume-length diameter does not give a good agreement with the experimental findings when considering particle velocity profiles.

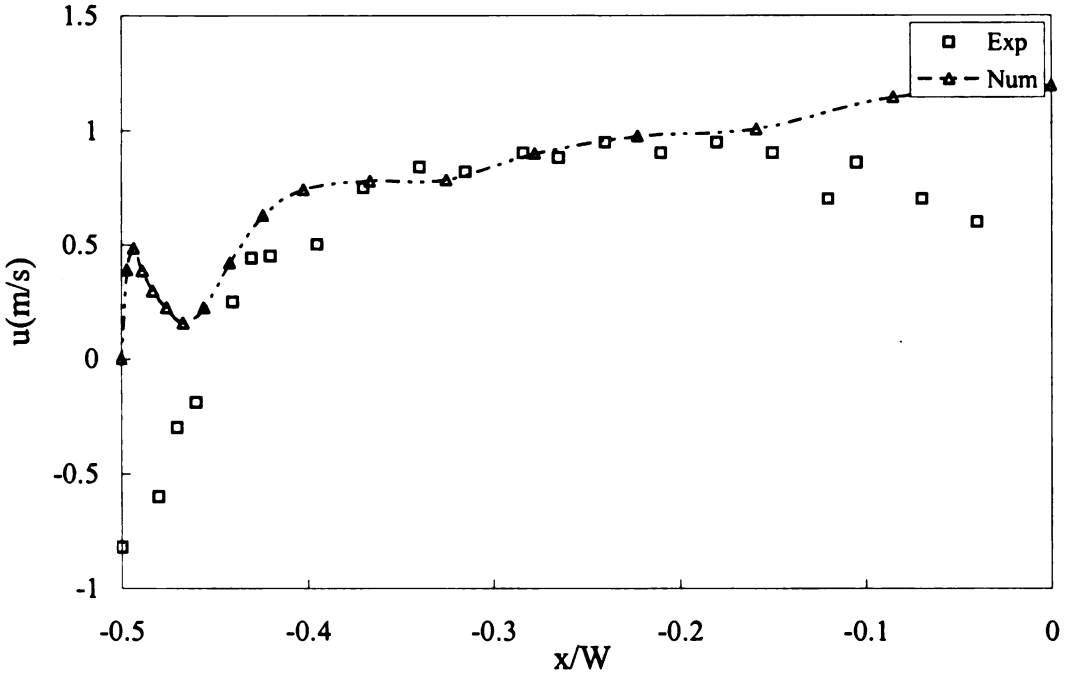

Figure 3.16: Plot of comparison between the measured (Ibsen et al., 2001) and computed axial particle velocities at profile 2. (x = 0 is the center of the duct).

The experimental findings in Figures 3.16 and 3.19 indicate a constant decrease in the axial and span wise velocities at the centerline whereas in the numerical model this trend for the particle velocities was not captured. Also in Figure 3.16 the predicted solid velocities near the wall deviate much from the experimental findings which are an indication that wall boundary conditions for the solid particles is quite complex.

In Figure 3.18, the particle velocities are not symmetric about the centre line which may indicate that the averaging time has been short. Also in Figure 3.19, the numerical predictions exhibit a rather poor match with the experiments.

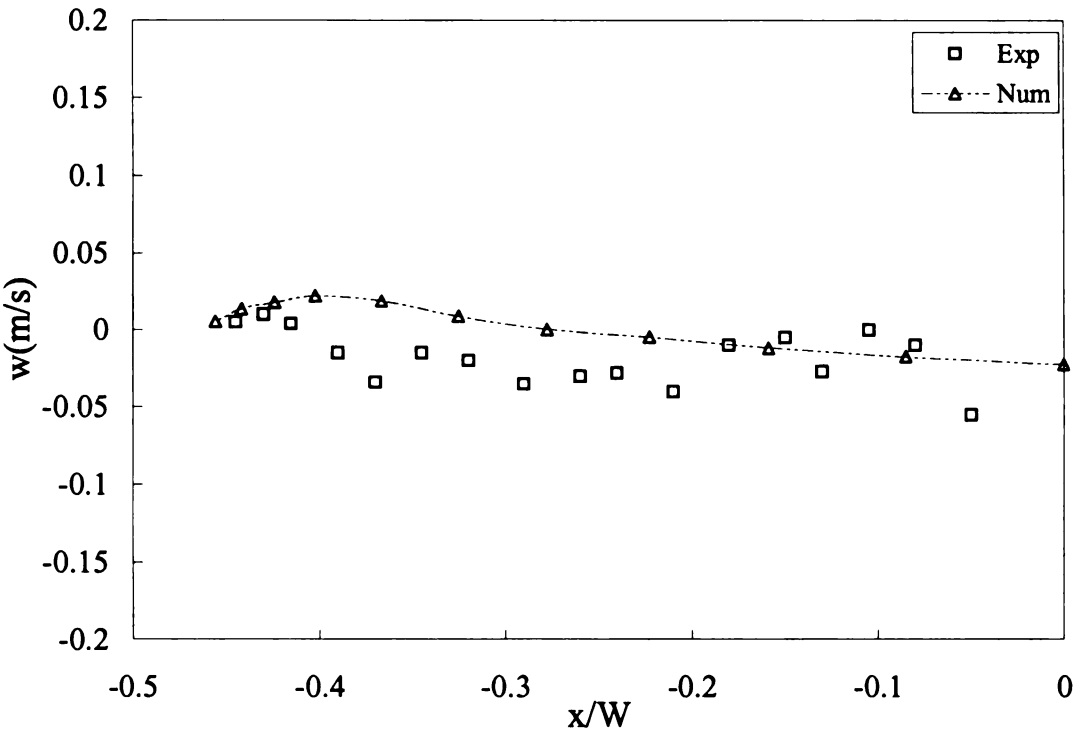

Figure 3.17: Plot of comparison between the measured (Ibsen et al., 2001) and computed span wise particle velocities at profile 2. (x = 0 is the center of the duct).

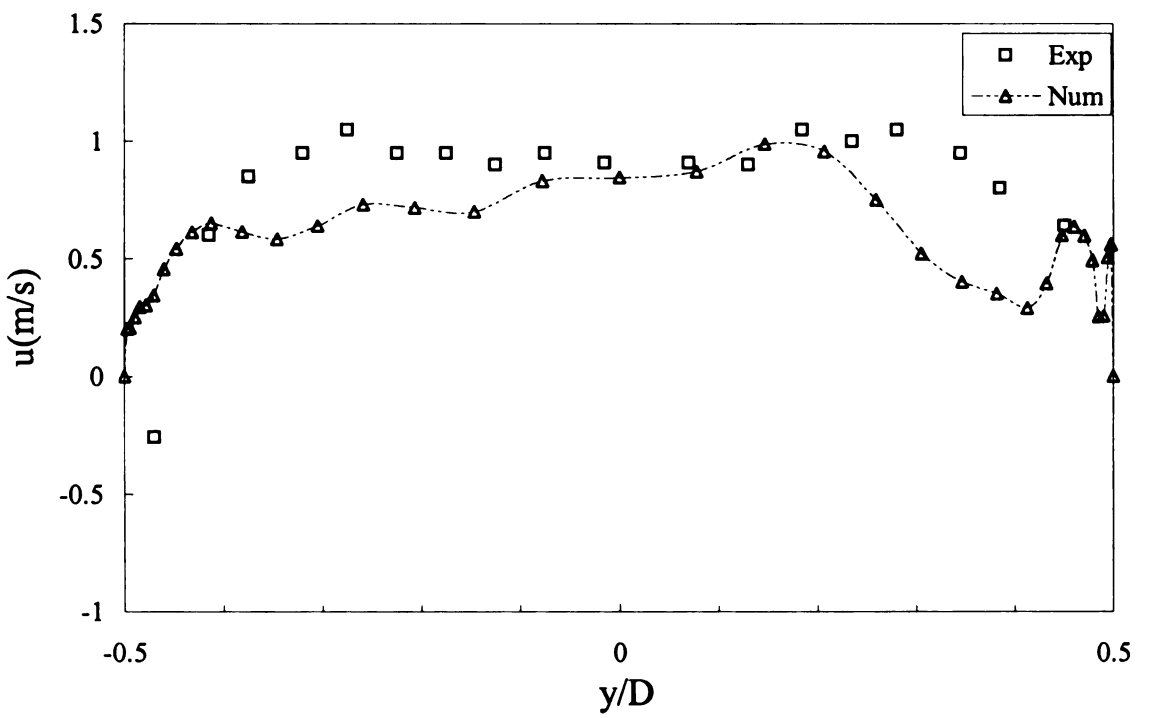

Figure 3.18: Plot of comparison between the measured (Ibsen et al., 2001) and computed axial particle velocities at profile 3.

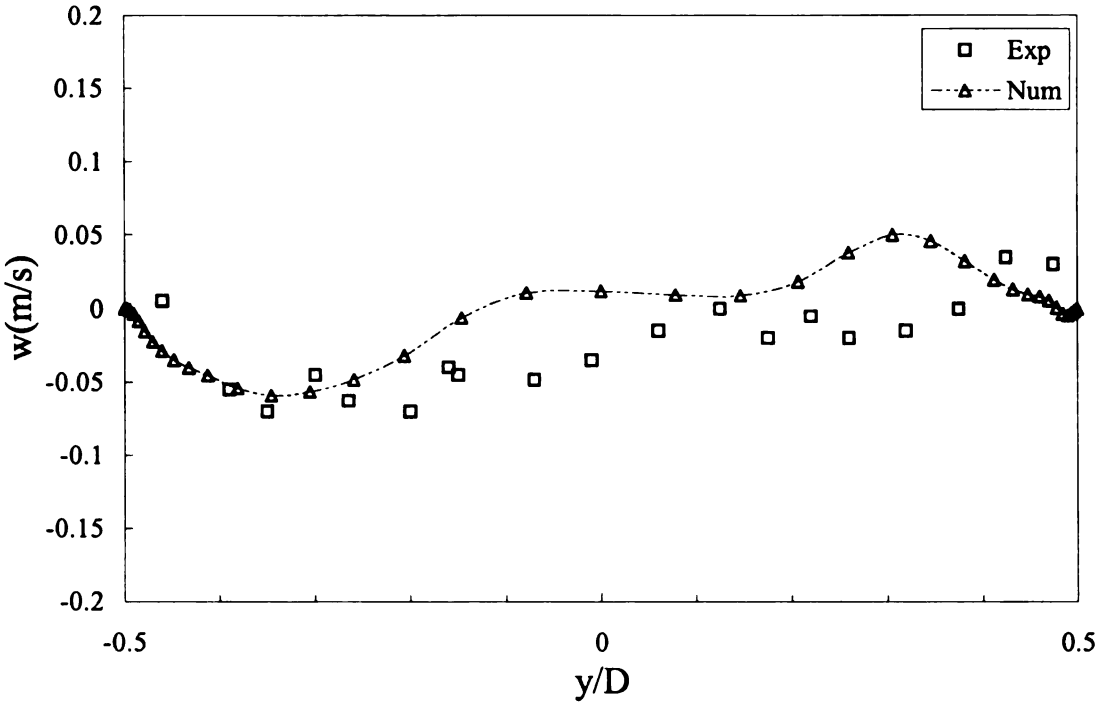

Figure 3.19: Plot of comparison between the measured (Ibsen et al., 2001) and computed span wise particle velocities at profile 3.

Volume fraction

Figures 3.20 and 3.21 present instantaneous contour plots of solids at various times and at various sections. The predicted time variation of the solids volumetric fraction through the riser of Circulating Fluidized Beds is indicative of a quite complex hydrodynamic behavior. There are steep variations on both span wise and axial solids concentrations, together with frequent formation and dissociation of clusters flowing both upwards and downwards. The numerical results show that fewer heavier simulated particles accumulate in the region very close to the wall due to larger inertia. Also, the simulations did not predict the dense bottom bed which was present in the experimental findings. The simulations predicted a mean solids volume fraction in the lowest part of the riser of 5-10 %. The solids volume fraction should have been 2-3 times higher. In addition, the simulations fail to capture the fine particles rather it shows the formation of clusters.

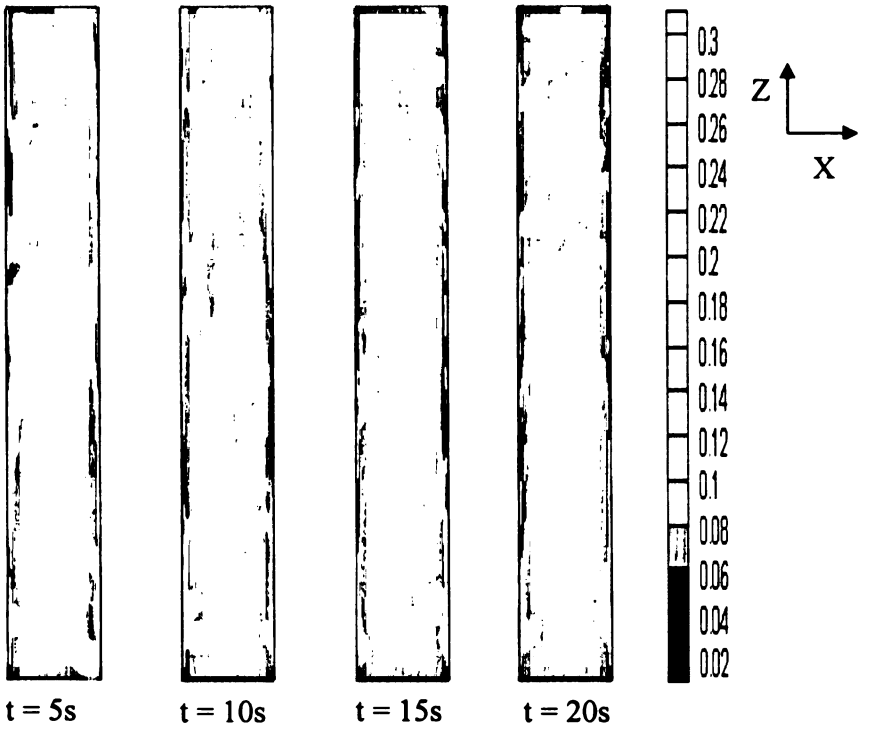

Figure 3.20: Contours of volume fraction of solids at various times for Y/D=0.

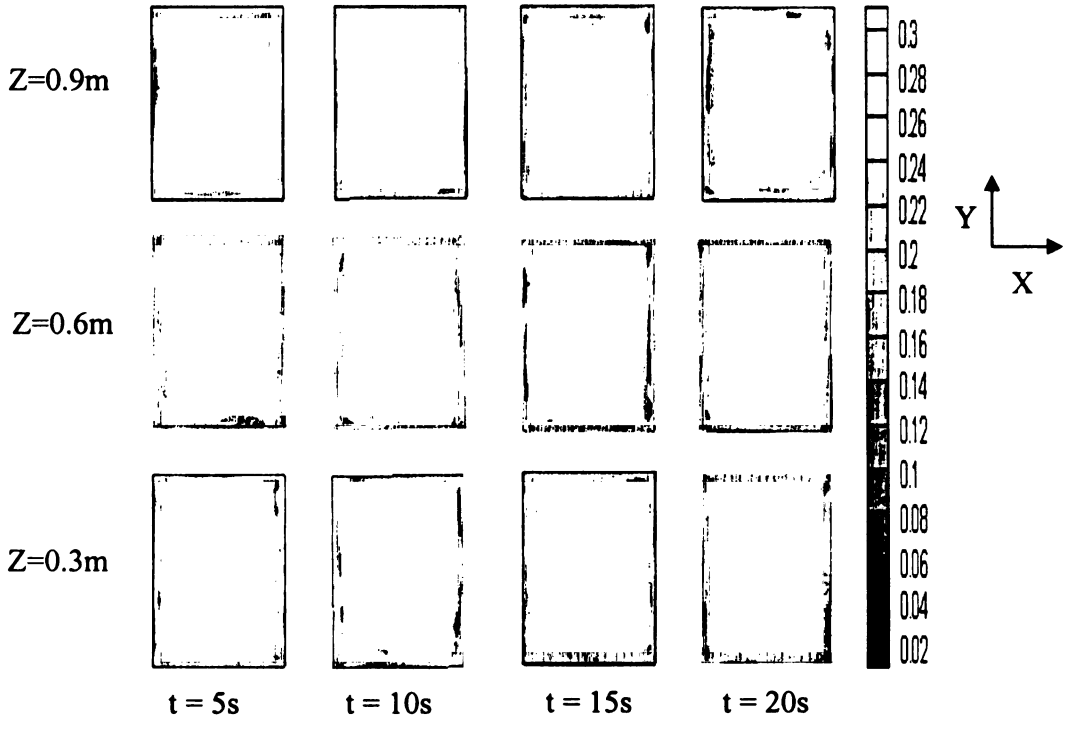

Figure 3.21: Contours of volume fraction of solids at various times for Z/H = -0.25, -0.5 and -0.75.

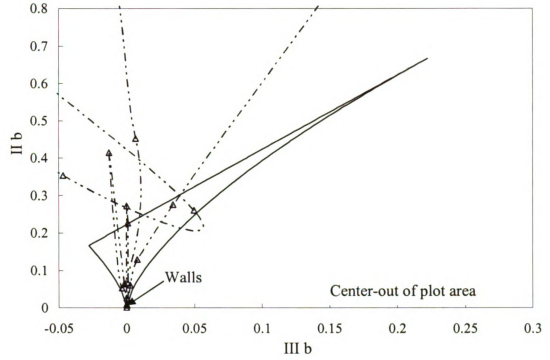

Figure 3.22: Realizability plot for the $\overline{u'u'}$ associated with the primary phase computed with the Realizable k - ε at profile 4.

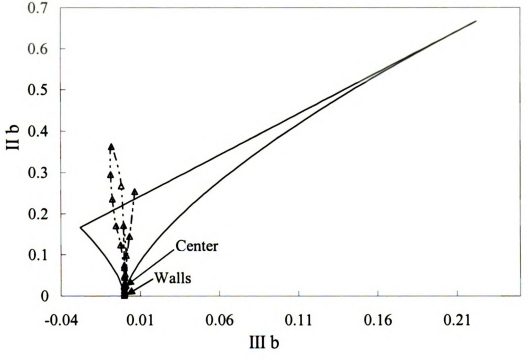

Figure 3.23: Realizability plot for the $\overline{u'u'}$ associated with the primary phase computed with the Realizable k - ε at profile 5.

The Realizability plots for the $\overline{\vec{u}'\vec{u}'}$ associated with the primary phase computed with the Realizable $k-\varepsilon$ is shown in Figures 3.22 and 3.23. In the two-phase simulations of gas-solid flows, the realizable $k-\varepsilon$ model proves to be highly unrealizable for the primary phase (air) near the center while it is realizable near the walls. The computed eigenvalues and invariants can be found in Tables C5 and C6 of Appendix C. Since the dispersed phase turbulence model is used in the simulations, the calculation of the eigenvalues and hence the realizability plot for the secondary phase (solids) is not possible.

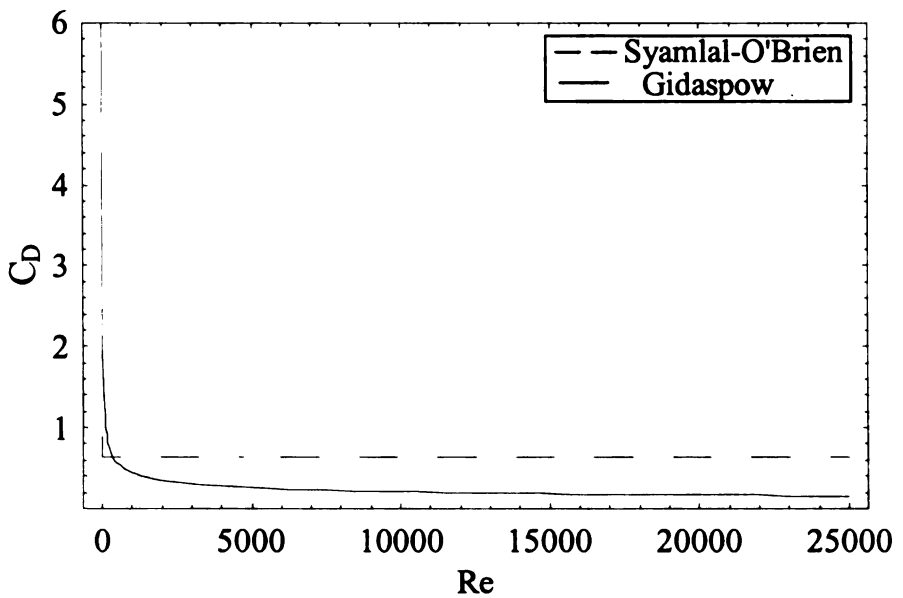

Figure 3.24: Plot of comparison of the two drag models for the gas-solid flows.

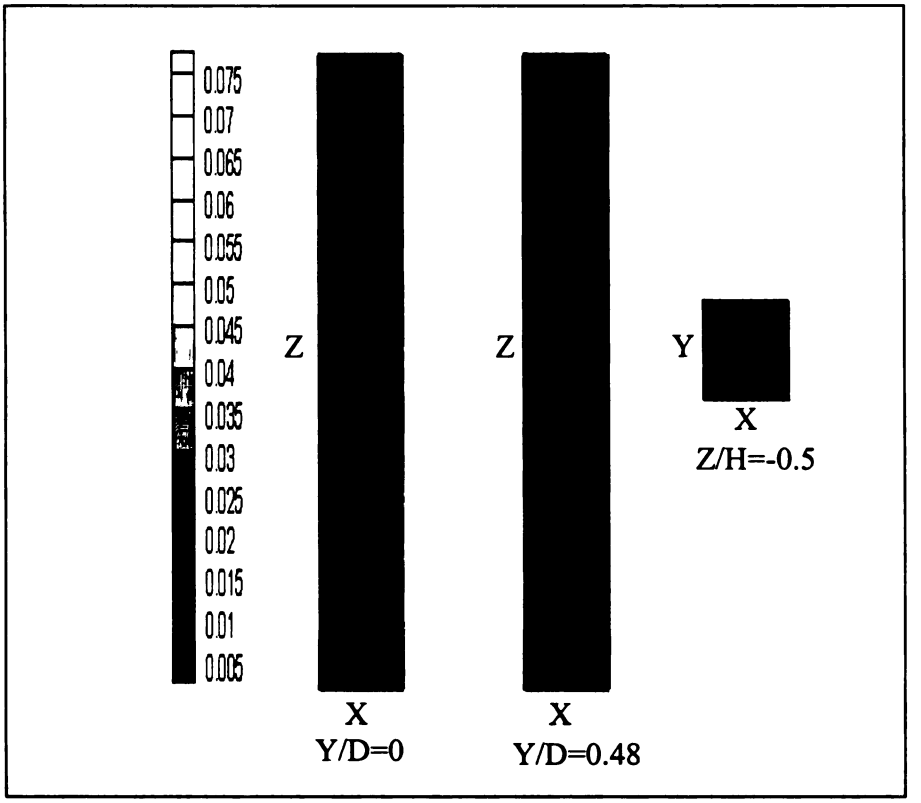

Figure 3.25: Contours of the turbulent kinetic energy for the primary phase (air) at Y/D=0, Y/D=0.8 and Z/H=-0.5.

Figure 3.25 shows that the contours of turbulent kinetic energy for the gas-solid simulations are the same at any cross-section in the riser.

CHAPTER 4

SUMMARY AND CONCLUSIONS

The objective of this work was to assess the performance of single phase flow and two-phase turbulent flow models implemented in FLUENT 6.2 using experiments and the invariant diagram for the Reynolds' stress. The Reynolds' stress must have positive or zero eigenvalues to be physical or realizable, and the invariant diagram bounds the region corresponding such eigenvalues.

Weakness observed in the models

The velocity vectors for the various turbulence models applied in the single phase flow simulations are the same except for the Reynolds Stress Model which predicted a great deviation from the other three viscous models. In addition, the various turbulence models proved to be realizable except for the Spalart-Allmaras model (Spalart et al., 1992) which showed to be unrealizable. Moreover, the Realizable k -ϵ model (Shih et al., 1995) which was realizable for single phase flows became very unrealizable for the primary phase in the two-phase flow simulations.

The gas-solid flow model was not able to predict the right order of pressure drop across the riser. Also, the predicted time averaged profiles of the axial and span wise particle velocities show good agreement with the experimental findings (Ibsen et al., 2001) only in some regions of the flow.

The gas-solid flow model is not capable of predicting the correct interaction of the turbulent gas phase and particles; the dispersion of the secondary phase is under predicted. The numerical results did not predict a dense bottom bed as seen in the experimental set-up. The simulations predicted a mean solids volume fraction in the

lowest part of the riser of 5-10 %. The solids volume fraction should have been 2-3 times higher.

Recommendations

The solid viscosity parameter and the interface momentum transfer applied should be rigorously modeled through a suitable theory which can accurately characterize the two-phase interactions and the physical phenomena involved. The kinetic theory of the granular flow is a promising theory for this purpose.

Turbulence effects must be accounted properly in gas-solid flows through Reynolds stress terms. According to Enwald et al. (1996), in bubbling fluidized beds which are characterized by high solids concentrations, the particulate inertia attenuates the gas phase turbulent parameters. However, for circulating fluidized beds which are mostly characterized by regions of low solids concentrations, turbulence becomes significant.

Since the gas-solid flows in fluidized beds are characterized by three-dimensional effects due to non-uniform shapes and sizes distributions of the particles, asymmetric solids feeding, asymmetric geometry at the exit of the riser, and the presence of solids separators such as cyclones, the whole installation should be simulated considering the above factors. Such simulations demand a very large number of grid cells in order to obtain grid independent solutions, which increase the computational time considerably. On the other hand, the uncertainty on the experimental measurements which are characteristic of gas-solids multiphase flows must be taken into account.

In summary, the results of simulation presented here strongly suggest that many features related to two-phase Eulerian approach needs improvement if accuracy is to be

achieved. Special attention should be directed towards interface momentum transfer, turbulence in two phases, pressure and viscosity of the secondary phase, and realistic boundary conditions. On the numerical side it becomes evident that more refined grids are required which unfortunately becomes prohibitive in view of the computational time.

APPENDICES

A. Models and near wall treatment applied in the thesis

Table A: Table summarizing the various turbulence models and the respective near wall treatments applied in the simulations along with their y^+ values.

Case	Turbulence Models	Near Wall Treatment	y^+	
Single Phase Turbulent Flow	Spalart-Allmaras	-	2.75	
	Standard $k-\omega$	-	2.6	
	Realizable $k-\varepsilon$	Standard Wall Treatment	2.75	
	Reynolds Stress Model	Enhanced Wall Treatment	2.6	
Bubbly Flow	Realizable $k-\varepsilon$	Enhanced Wall Treatment	Air	0.66
			Water	9.25
Gas-solid Flow	Realizable $k-\varepsilon$	Enhanced Wall Treatment	Air	9.8
			Solid	18

B: Comparison of terms for the various turbulent viscous models.

Table B1: Table summarizing the various terms for the Spalart-Allmaras model and the Standard $k-\omega$ model studied.

Terms	Turbulence Closure Models	
	Spalart-Allmaras	**Standard $k-\omega$**
Local Time Derivative	$\frac{\partial}{\partial t}(\rho\bar{\nu})$	$\frac{\partial}{\partial t}(\rho k)$; $\frac{\partial}{\partial t}(\rho\omega)$
Convection	$\frac{\partial}{\partial x_j}(\rho\bar{\nu}u_j)$	$\frac{\partial}{\partial x_j}(\rho k u_j)$; $\frac{\partial}{\partial x_j}(\rho\omega u_j)$
Turbulent Viscosity	$\mu_t = \rho\bar{\nu}f_{v1}$	$\mu_t = \frac{\alpha^*\rho k}{\omega}$
Production terms	$G_\nu = C_{b1}\rho\bar{S}\bar{\nu}$	$\frac{2\mu_t}{\sigma_k}S_{ij}S_{ij}$; $2\frac{\alpha\omega}{k}\mu_t S_{ij}S_{ij}$
Dissipation terms	-	$\rho\beta^* f_{\beta^*} k\omega$; $\rho\beta f_\beta \omega^2$
Destruction terms	$Y_\nu = C_{w1}\rho f_w\left(\frac{\bar{\nu}}{d}\right)^2$	-

Table B2: Table summarizing the various terms for the Realizable $k-\varepsilon$ model and the Reynolds Stress model studied.

Terms	Turbulence Closure Models	
	Realizable $k-\varepsilon$	**Reynolds Stress Model**
Local Time Derivative	$\frac{\partial}{\partial t}(\rho k)$; $\frac{\partial}{\partial t}(\rho\varepsilon)$	$\frac{\partial}{\partial t}\left(\rho\overline{\vec{u}_i'\vec{u}_j'}\right)$
Convection	$\frac{\partial}{\partial x_j}(\rho k u_j)$; $\frac{\partial}{\partial x_j}(\rho\varepsilon u_j)$	$\frac{\partial}{\partial x_k}\left(\rho\vec{U}_k\overline{\vec{u}_i'\vec{u}_j'}\right)$
Turbulent Viscosity	$\mu_t = \rho C_\mu\frac{k^2}{\varepsilon}$	-
Production terms	$\frac{2\mu_t}{\sigma_k}S_{ij}S_{ij}$; $\rho C_1\varepsilon\sqrt{2S_{ij}S_{ij}}$	$-\rho\left(\overline{\vec{u}_i'\vec{u}_k'}\frac{\partial\vec{u}_j'}{\partial x_k}+\overline{\vec{u}_j'\vec{u}_k'}\frac{\partial\vec{u}_i}{\partial x_k}\right)$; $-\rho\beta\left(g_i\overline{\vec{u}_j'\theta}+g_j\overline{\vec{u}_i'\theta}\right)$; $-2\rho\Omega_k\left(\overline{\vec{u}_j'\vec{u}_m'}\varepsilon_{ikm}+\overline{\vec{u}_i'\vec{u}_m'}\varepsilon_{jkm}\right)$
Dissipation terms	$\rho\varepsilon$; $\rho C_2\frac{\varepsilon^2}{k+\sqrt{\nu\varepsilon}}$	$2\mu\overline{\frac{\partial\vec{u}_i'}{\partial x_k}\frac{\partial\vec{u}_j'}{\partial x_k}}$
Destruction terms	$D_\varepsilon = C_{1\varepsilon}\frac{\varepsilon}{k}C_{3\varepsilon}G_b$	-

C. Computed eigenvalues and invariants

Table C1: Computed eigenvalues and invariants for a single phase turbulent flow using the Spalart-Allmaras model; Y/D=0; Z/H=-0.5

Location	Eigenvalues			Invariants	
X	λ_1	λ_2	λ_3	II_b	III_b
-0.085	-14456.1	-0.057	14457.12	4.18E+08	2.45E+08
-0.0845	-59086.6	0.635	59087	6.98E+09	-3.2E+09
-0.08388	-17465.2	0.586	17465.59	6.1E+08	-2.3E+08
-0.08309	-50871.3	-4.2	50876.46	5.18E+09	3.52E+10
-0.08212	-119145	-23.62	119169.3	2.84E+10	1.02E+12
-0.0809	-18093.2	-8.5	18102.7	6.55E+08	8.67E+09
-0.07937	-123432	127.45	123305.7	3.04E+10	-5.8E+12
-0.07746	-24271.1	-49.84	24321.95	1.18E+09	8.89E+10
-0.07508	-5700.57	21.84	5679.73	64756219	-2.1E+09
-0.0721	-3055.86	21.55	3035.31	18551858	-5.9E+08
-0.06837	-1033.24	-14.7	1048.93	2168052	48864675
-0.06231	-1070.94	63.76	1008.17	2167373	-2.1E+08
-0.0553	-41.1141	-37.3	79.4	9383.897	369801.2
-0.0472	-363.45	154.5	209.9	200040	-3.5E+07
-0.03783	-989.754	-571.25	1562	3745782	2.65E+09
-0.027	-2164.92	888.26	1277.6	7108310	-7.4E+09
-0.01448	-1586.92	-1352.79	2940.7	12996163	1.89E+10
2.22E-18	-1748.73	844.1941	905.5	4590694	-4E+09
0.014479	-1586.92	-1352.79	2940.7	12996163	1.89E+10
0.027002	-2170.92	890.717	1281.2	7147756	-7.4E+09
0.037834	-989.754	-571.25	1562	3745782	2.65E+09
0.047202	-363.45	154.54	209.9	200040	-3.5E+07
0.055304	-41.1141	-37.28	79.4	9383.897	369801.2
0.062312	-1070.94	63.76	1008.17	2167373	-2.1E+08
0.068374	-1033.24	-14.7	1048.9	2168052	48864675
0.072099	-3053.71	21.54	3033.2	18525687	-5.9E+08
0.075079	-5700.57	21.84	5679.73	64756219	-2.1E+09
0.077463	-24271.1	-49.84	24321.95	1.18E+09	8.89E+10
0.079371	-123432	127.45	123305.7	3.04E+10	-5.8E+12
0.080897	-18093.2	-8.49	18102.7	6.55E+08	8.67E+09
0.082117	-119145	-23.62	119169.3	2.84E+10	1.02E+12
0.083094	-50871.3	-4.2	50876.46	5.18E+09	3.52E+10
0.083875	-17465.2	0.58	17465.6	6.1E+08	-2.3E+08
0.0845	-59086.6	0.63	59087	6.98E+09	-3.2E+09
0.085	-14456.1	-0.056	14457.12	4.18E+08	2.45E+08

Table C2: Computed eigenvalues and invariants for a single phase turbulent flow using the Spalart-Allmaras model; Y/D=0.48; Z/H=-0.5

Location	Eigenvalues			Invariants	
X	λ_1	λ_2	λ_3	II_b	III_b
-0.085	-11377.2	0.543	11377.65	258891356	-81437229
-0.0845	-73150.8	-7.171	73159.01	1.07E+10	1.2E+11
-0.08388	-17592.8	-3.828	17597.59	619180587	3.86E+09
-0.08309	-68104.8	23.31	68082.51	9.273E+09	-3.2E+11
-0.08212	-49683.2	-21.29	49705.47	4.939E+09	1.6E+11
-0.0809	-106722	-51.75	106774.9	2.279E+10	1.78E+12
-0.07937	-95947.7	-45.28	95993.98	1.842E+10	1.26E+12
-0.07746	-671307	-265.1	671573.3	9.017E+11	3.59E+14
-0.07508	-373809	91.76	373717.9	2.794E+11	-3.83E+13
-0.0721	-107809	6.227	107803.4	2.324E+10	-2.05E+11
-0.06837	-44903.7	-4.903	44909.57	4.033E+09	3.17E+10
-0.06231	-70731.2	-14.15	70746.37	1.001E+10	2.17E+11
-0.0553	-80329.6	-14.57	80345.19	1.291E+10	2.89E+11
-0.0472	-98622	-17.45	98640.47	1.946E+10	5.19E+11
-0.03783	-93456.7	-17.1	93474.76	1.747E+10	4.57E+11
-0.027	-113695	-20.63	113717.1	2.586E+10	8.13E+11
-0.01448	-114072	-21.13	114094.2	2.603E+10	8.38E+11
2.22E-18	-109972	-20.68	109993.7	2.419E+10	7.63E+11
0.014479	-114072	-21.13	114094.2	2.603E+10	8.38E+11
0.027002	-113717	-20.63	113738.4	2.587E+10	8.14E+11
0.037834	-93456.7	-17.1	93474.76	1.747E+10	4.57E+11
0.047202	-98622	-17.45	98640.47	1.946E+10	5.19E+11
0.055304	-80329.6	-14.57	80345.19	1.291E+10	2.89E+11
0.062312	-70731.2	-14.15	70746.37	1.001E+10	2.17E+11
0.068374	-44903.7	-4.903	44909.57	4.033E+09	3.17E+10
0.072099	-107809	6.227	107803.4	2.324E+10	-2.05E+11
0.075079	-373809	91.76	373717.9	2.794E+11	-3.83E+13
0.077463	-671307	-265.1	671573.3	9.017E+11	3.59E+14
0.079371	-95947.7	-45.28	95993.98	1.842E+10	1.26E+12
0.080897	-106722	-51.75	106774.9	2.279E+10	1.78E+12
0.082117	-49683.2	-21.29	49705.47	4.939E+09	1.6E+11
0.083094	-68104.8	23.31	68082.51	9.273E+09	-3.2E+11
0.083875	-17592.8	-3.828	17597.59	619180587	3.86E+09
0.0845	-73150.8	-7.171	73159.01	1.07E+10	1.2E+11
0.085	-11377.2	0.543	11377.65	258891356	-81437229

Table C3: Computed eigenvalues and invariants for the primary phase (water) in the gas-liquid simulations; Y/D=0; Z/H=-0.5

Location	Eigenvalues			Invariants	
X	λ_1	λ_2	λ_3	II_b	III_b
-0.085	-15.314	0.333	15.981	489.71	0.100727
-0.0845	-78.501	0.331	79.17	12430.05	37.72916
-0.08388	-84.027	0.321	84.706	14235.27	261.2749
-0.08309	-83.944	0.292	84.652	14212.32	883.6041
-0.08212	-91.626	0.246	92.379	16928.98	2205.522
-0.0809	-97.869	0.172	98.697	19319.07	4666.574
-0.07937	-102.23	0.057	103.17	21093.31	8747.825
-0.07746	-102.14	-0.105	103.25	21092.16	13874.94
-0.07508	-96.931	-0.282	98.214	19041.36	17578.25
-0.0721	-89.106	-0.469	90.574	16143.41	19416.09
-0.06837	-88.54	-0.937	90.478	16026.11	30537.17
-0.06231	-73.806	-2.816	77.622	11480.15	54144.5
-0.0553	-33.228	-4.739	38.967	2644.666	19730.94
-0.0472	-20.715	-11.24	32.957	1641.359	23846.03
-0.03783	-14.21	-11.94	27.151	1081.379	14362.18
-0.027	-18.418	-18.12	37.541	2076.644	38630.16
-0.01448	-80.805	-76.15	157.95	37277.11	2934399
2.22E-18	-349.24	166.9	183.31	183435.4	-3.2E+07
0.014479	-80.805	-76.15	157.95	37276.86	2934369
0.027002	-18.418	-18.12	37.541	2076.633	38629.85
0.037834	-14.21	-11.94	27.151	1081.366	14361.94
0.047202	-20.714	-11.24	32.955	1641.089	23839.91
0.055304	-33.227	-4.739	38.966	2644.532	19729.05
0.062312	-73.805	-2.816	77.621	11479.7	54139.79
0.068374	-88.54	-0.937	90.477	16026.04	30536.01
0.072099	-89.105	-0.469	90.574	16143.19	19415.11
0.075079	-96.931	-0.282	98.214	19041.36	17577.63
0.077463	-102.14	-0.105	103.25	21092.16	13874.41
0.079371	-102.22	0.057	103.17	21093.26	8747.404
0.080897	-97.869	0.172	98.697	19319.07	4666.31
0.082117	-91.626	0.246	92.379	16928.96	2205.372
0.083094	-83.944	0.292	84.652	14212.31	883.5298
0.083875	-84.027	0.321	84.705	14235.25	261.2384
0.0845	-78.501	0.331	79.17	12430.05	37.71271
0.085	-15.314	0.333	15.981	489.71	0.100622

Table C4: Computed eigenvalues and invariants for the primary phase (water) in the gas-liquid simulations; Y/D=0.48; Z/H=-0.5

Location	Eigenvalues			Invariants	
X	λ_1	λ_2	λ_3	II_b	III_b
-0.085	-10.07	0.33	10.7	216.36	-0.23
-0.0845	-59.8	0.34	60.47	7234.09	-107.13
-0.08388	-72.67	0.38	73.28	10649.64	-741.163
-0.08309	-83.76	0.47	84.3	14121.98	-2840.333
-0.08212	-95.94	0.6	96.36	18490	-6826.123
-0.0809	-95.86	0.6	96.22	18449.4	-8452.243
-0.07937	-88.062	0.65	88.4	15572	-7364.19
-0.07746	-85.38	0.65	85.7	14639.8	-6942.07
-0.07508	-86.43	0.64	86.8	15004.78	-6806.9
-0.0721	-87.73	0.6	88.13	15463	-6115.5
-0.06837	-89.6	0.52	90.07	16137.8	-4517.27
-0.06231	-92.26	0.4	92.9	17138.43	-1239.33
-0.0553	-92.7	0.28	93.47	17339.98	1437.67
-0.0472	-93.9	0.23	94.68	17784.64	2850.82
-0.03783	-93.7	0.22	94.51	17718.58	2972.55
-0.027	-93.58	0.23	94.35	17659.59	2795.52
-0.01448	-93.9	0.22	94.67	17778.62	2871.7
2.22E-18	-93.9	0.22	94.73	17800.57	2979.48
0.014479	-93.9	0.22	94.67	17778.53	2871.57
0.027002	-93.58	0.23	94.35	17659.45	2795.08
0.037834	-93.7	0.22	94.51	17718.62	2971.63
0.047202	-93.9	0.23	94.67	17780.68	2844.21
0.055304	-92.77	0.28	93.49	17345.67	1432.34
0.062312	-92.24	0.38	92.86	17132.51	-1222.6
0.068374	-89.6	0.52	90.09	16146.75	-4511.6
0.072099	-87.75	0.6	88.15	15470.52	-6134.7
0.075079	-86.42	0.6	86.78	14999.34	-6818.45
0.077463	-85.37	0.65	85.73	14638.62	-6949
0.079371	-88.06	0.65	88.4	15572.18	-7370.8
0.080897	-95.87	0.64	96.23	18450.72	-8460
0.082117	-95.95	0.58	96.36524	18491.7	-6833.8
0.083094	-83.77	0.47	84.3012	14123.8	-2845
0.083875	-72.67	0.38	73.28319	10650	-741
0.0845	-59.8	0.34	60.47115	7234.3	-107.4
0.085	-10.07	0.33	10.73	216.3	-0.23

Table C5: Computed eigenvalues and invariants for the primary phase (air) in the gas-solid simulations; Y/D=0; Z/H=-0.5.

Location	Eigenvalues			Invariants	
X	λ_1	λ_2	λ_3	II_b	III_b
-0.085	0.33	0.33	0.34	4.86E-05	-2.1E-09
-0.0845	0.33	0.33	0.34	2.74E-05	-9.5E-10
-0.08388	0.31	0.33	0.354	0.000998	1.28E-07
-0.08309	0.27	0.33	0.44	0.009	8.02E-06
-0.08212	0.28	0.328	0.4	0.0067	4.93E-05
-0.0809	0.15	0.35	0.54	0.0632	-0.00172
-0.07937	-0.13	0.35	0.774	0.4	-0.0126
-0.07746	0.15	0.38	0.464	0.05	-0.00345
-0.07508	-0.14	0.323	0.84	0.45	0.007
-0.0721	-0.57	0.375	1.1954	1.56	-0.098
-0.06837	-0.99	0.475	1.517	3.18	-0.67
-0.06231	-0.6	0.58	1.02	1.41	-0.48
-0.0553	-0.125	0.42	0.7	0.35	-0.047
-0.0472	0.078	0.175	0.7	0.26	0.05
-0.03783	-0.82	0.487	1.33	2.36	-0.53
-0.027	-1.99	0.458	2.54	10.34	-1.93
-0.01448	-7.62	0.315	8.3	126.68	3.37
2.22E-18	-6.6	-1.03	8.6	119.6	236.7
0.014479	-3.12	-0.71	4.8	33.24	48.79
0.027002	-2.32	0.11	3.2	15.3	4.998
0.037834	-0.67	0.43	1.24	1.85	-0.26
0.047202	-0.8	0.24	1.55	2.78	0.4
0.055304	-0.8	0.205	1.59	2.86	0.54
0.062312	0.014	0.24	0.74	0.27	0.034
0.068374	0.103	0.3	0.6	0.13	0.008
0.072099	0.18	0.3	0.52	0.06	0.002749
0.075079	0.25	0.3	0.45	0.02	0.001082
0.077463	0.15	0.32	0.52	0.07	0.001068
0.079371	-0.00179	0.33	0.671	0.23	0.000976
0.080897	-0.035	0.33	0.7	0.27	0.000129
0.082117	0.218	0.33	0.45	0.03	-8.4E-06
0.083094	0.32	0.33	0.34	0.000135	5E-08
0.083875	0.314	0.33	0.35	0.000758	2.13E-07
0.0845	0.33	0.33	0.33	1.21E-05	4.02E-10
0.085	0.33	0.33	0.34	7.89E-05	2.34E-09

Table C6: Computed eigenvalues and invariants for the primary phase (air) in the gas-solid simulations; Y/D=0.48; Z/H=-0.5.

Location	Eigenvalues			Invariants	
X	λ_1	λ_2	λ_3	II_b	III_b
-0.085	0.33	0.333	0.336	1.7E-05	1.24E-10
-0.0845	0.333	0.333	0.334	7.54E-08	-8.4E-13
-0.08388	0.291	0.333	0.376	0.003595	-6.8E-07
-0.08309	0.224	0.335	0.441	0.023593	-4.9E-05
-0.08212	0.173	0.329	0.499	0.053186	0.000362
-0.0809	-0.014	0.316	0.698	0.254016	0.006552
-0.07937	0.072	0.318	0.61	0.145081	0.00332
-0.07746	0.139	0.335	0.527	0.07531	-0.00014
-0.07508	0.293	0.34	0.367	0.002817	-2.6E-05
-0.0721	0.236	0.306	0.458	0.025795	0.000996
-0.06837	0.115	0.326	0.559	0.098595	0.001086
-0.06231	0.04	0.335	0.625	0.171139	-0.00037
-0.0553	0.147	0.334	0.519	0.069209	-9.2E-05
-0.0472	0.207	0.333	0.46	0.031912	3.08E-05
-0.03783	0.223	0.333	0.444	0.024254	8.41E-06
-0.027	0.231	0.335	0.435	0.020864	-4.1E-05
-0.01448	0.246	0.337	0.418	0.014756	-7.2E-05
2.22E-18	0.25	0.34	0.41	0.012965	-0.00013
0.014479	0.22	0.338	0.442	0.024735	-0.00019
0.027002	0.184	0.332	0.485	0.045323	0.000121
0.037834	0.258	0.325	0.417	0.012773	0.000156
0.047202	0.269	0.333	0.398	0.008434	2.89E-06
0.055304	0.285	0.332	0.383	0.004827	6.23E-06
0.062312	0.229	0.325	0.446	0.023592	0.000278
0.068374	-0.035	0.338	0.697	0.267441	-0.00188
0.072099	-0.1	0.348	0.752	0.362615	-0.00795
0.075079	-0.06	0.353	0.708	0.295388	-0.00863
0.077463	-0.02	0.355	0.666	0.235889	-0.00753
0.079371	0.032	0.354	0.614	0.17037	-0.00526
0.080897	0.079	0.346	0.575	0.123601	-0.0024
0.082117	0.176	0.334	0.489	0.049053	-7.9E-05
0.083094	0.27	0.329	0.401	0.008565	5.35E-05
0.083875	0.293	0.333	0.374	0.003315	2.55E-06
0.0845	0.332	0.333	0.334	2.52E-06	7.1E-11
0.085	0.331	0.333	0.336	1.18E-05	3.91E-10

REFERENCES

Agrawal K., Peter N. Loezos, Syamlal M. and Sundaresan S., 2001, "The Role of Meso-Scale Structures in Rapid Gas-Solid Flows", J. Fluid Mech., Vol. 445, pp.151-185.

Arthur T. A. IV, Peter N. L. and Sundaresan S., 2005, "Coarse-Grid Simulation of Gas-Particle Flows in Vertical Risers", Ind. Eng. Chem. Res., 44 (16), 6022 -6037.

Balzer G., and Simonin O., 1997, "Three dimensional numerical predictions of two phase flow in industrial CFB boiler", In: *14.* International conference on fluidized bed combustion, Vancouver, Br. C.. Vol. 2. ASME. pp. 1017–1022.

Benyahia S., Arastoopour H. and Knowlton T. M., 2002, "Two-Dimensional Transient Numerical Simulation of Solids and Gas Flow in the Riser Section of a Circulating Fluidized Bed", Chem. Eng. Comm., Vol. 189(4).

Benyahia S., Arastoopour H., Knowlton T. M. and Massah H., "Simulation of Particles and Gas Flow Behavior in the Riser Section of a Circulating Fluidized Bed Using the Kinetic Theory Approach for the Particulate Phase", Accepted for publication in Powder Technology.

Benyahia S., Arastoopour H., Knowlton T. M., 1999, "Three-dimensional transit numerical simulation of solids and gas flow in the riser section of a circulating fluidized bed" in Glicksman L. R. (Ed.), Fluidization and Fluid-Particle Systems, AIChE, Dallas, TX. 33-40.

Benyahia S., Arastoopour H., Knowlton T. M. and Massah H., 2000, "Simulation of Particles and Gas Flow Behavior in the Riser Section of a Circulating Fluidized Bed Using the Kinetic Theory Approach for the Particulate Phase", Powder Technology 112, 24–33.

Berkelmann K.G., and Renz U., 1991, "Gas and solid flow in the freeboard of a fluidized bed combustor", Powder Technology 68, 271–280.

Bjorn H. H., Solberg T. and Kim G. H., 2005, "Reactive Gas Solids Flow in Circulating Fluidized Beds", Fourth International Conference on CFD in the Oil and Gas, Metallurgical & Process Industries, SINTEF / NTNU Trondheim, Norway.

Bouillard J. X., 1989, "Porosity distributions in a fluidized bed with an immersed obstacle", AIChE Journal, Vol.35, no.6, pp.908-922.

Boussinesq, J., 1877, "Essai sur la theories des eaux courantes," Mémoires présentés par divers savants a l'Académie des Sciences de l'Institut National de France, 23(1).

Chapman S., and Cowling T. G., 1970, "The Mathematical Theory of Non-Uniform Gases", 3 ed. Cambridge University Press.

Chen C.J and Jaw S. Y., c1998, "Fundamentals of turbulence modeling", Washington, DC: Taylor & Francis.

Constantinescu V. N., 1995, "Laminar Viscous Flow", Springer-Verlag, New York.

Deen, N.G., Solberg T. and Hjertager B.H., 2001, "Large Eddy Simulation of the Gas-Liquid Flow in a Square Cross-sectioned Bubble Column", GLS5, 5th Int. Conf. on Gas-Liquid and Gas-Solid-Liquid Reactor Engineering, Melbourne, Australia.

De Wilde, Juray, Vierendeels J., Heynderickx G. J., and Marin G. B., 2001, "An extension of the preconditioned advection upstream splitting method to two-phase flows for the 3D calculation of circulating fluidized bed flow patterns", In: 3rd International Symposium on Computational Technologies for Fluid/Chemical Systems with Industrial Applications. ASME.

Ding, Jianmin and Gidaspow D., 1990, "A bubbling fluidization model using kinetic theory of granular flow", AIChE J. 36(4), 523–538.

Enwald H., and Almstedt A. E., 1999, "Fluid dynamics of a pressurized fluidized bed: comparison between numerical solutions from two-fluid models and experimental results", Chem. Eng. Sci. 54, 329–342.

Enwald H., Peirano E., and Almstedt A. E., 1996, "Eulerian two-phase flow theory applied to fluidization", Int. J. Multiphase Flow 22, 21–66.

Ergun S., 1952, "Fluid Flow through Packed Columns", Chem. Eng. Prog, 48(2):89-94.

Fluent 6.2, User's Guide, Fluent Incorporated, Lebanon, NH.

Gibson M. M. and Launder B. E., 1978, "Ground Effects on Pressure Fluctuations in the Atmospheric Boundary Layer", J. Fluid Mech., 86:491-511.

Gidaspow D., 1994, "Multiphase Flow and Fluidization", Academic Press, Inc., U.K.

Gidaspow D., Bezburuah R., and Ding J., 1992, "Hydrodynamics of circulating fluidized beds: Kinetic theory approach", In: Fluidization VII (O. E. Potter, Ed.). Engineering Foundation. New York. pp. 75–82.

Gidaspow D., 1986, "Hydrodynamics of fluidization and heat transfer: Supercomputer modeling", Appl. Mech. Rev. 39(1), 1–23.

Gidaspow D., Bezburuah R., and Ding J., 1992, "Hydrodynamics of Circulating Fluidized Beds, Kinetic Theory Approach", In Fluidization VII, Proceedings of the 7th Engineering Foundation Conference on Fluidization, pages 75-82.

Gidaspow D. and Ettehadieh B., 1983, "Fluidization in two-dimensional beds with a jet. 2. Hydrodynamics modeling", I & EC Fundam., Vol.22, pp.193-201.

Gidaspow D., 1994, "Multiphase Flow and Fluidization", Academic Press, Inc.
Gillandt I., Fritsching U., and Bauckhage K., 2001, "Measurement of two phase interaction in dispersed gas-particle two-phase flow", Int. J. Multiphase Flow 27, 1313–1332.

Harris Pugsley T.S. and Berruti F., 1996, "A predictive model for circulating fluidized bed risers", Powder Technology, v.89, p.57-69.

Hamdullahpur F., Pegg M. J., and MacKay G. D. M., 1987, "A laser fluorescence technique for turbulent two-phase flow measurements", Int. J. Multiphase flow 13(3), 379–385.

Helland, Eivind, Occelli R and Tadrist L., 2002, "Computational study of fluctuating motions and cluster structures in gas-particle flows", Int. J. Multiphase Flow 28, 199–223.

Helland, Eivind, Ocelli R and Tadrist L., 2000, "Numerical study of cluster formation in a gas-particle circulating fluidized bed", Powder Technology 110, 210–221.

Hinze J.O., 1975, "Turbulence", McGraw-Hill Publishing Co., New York.

Hoomans B. P. B., Kuipers J. A. M., and Van Swaaij W. P. M., 2000, "Granular dynamics simulation of segregation phenomena in bubbling gas-fluidised beds", Powder Technology 109, 41–48.

Hoomans B. P. B., Kuipers J. A. M., Briels W. J. and Van Swaaij W. P. M., 1996, "Discrete particle simulation of bubble and slug formation in a two-dimensional gas-fluidised bed: A hard sphere approach", Chem. Eng. Sci. 51(1), 99–118.

Hutchinson B. R. and Raithby G. D., 1986, "A Multigrid Method Based on the Additive Correction Strategy, Numerical Heat Transfer", 9:511-537.

Ibsen C.H., Solberg T. and Hjertager B.H., 2001, "Evaluation of a Three-Dimensional Numerical Model of a Scaled Circulating Fluidized Bed", Industrial & Engineering Chemistry Research, Vol. 40, no. 23, pp. 5081-5086.

Ibsen C.H., Hjertager B.H., Solberg T. and Johnsson F., 2001, "Laser Doppler Anemometry Measurements in a Circulating Fluidized Bed of Metal Particles", ICMF-2001, 4th International Conference on Multiphase Flow, May 27 - June 1 2001, New Orleans, Louisiana, USA.

Jenkins J.T. and Richman, M.W., 1985, "Grad's 13 moment system for a dense gas of inelastic spheres", Archive for Rational Mechanics and Analysis, Vol.87, no.4, pp.355-377.

Jenkins J. T. and Mancini F., 1987, "Balance laws and constitutive relations for plane flows of a dense mixture of smooth, nearly elastic, circular disks", J. App. Mech. 54, 27–34.

Jenkins, J. T. and Savage S. B., 1983, "A theory for the rapid flow of identical, smooth, nearly elastic, spherical particles", J. Fluid Mech. 130, 187–202.

Johnsson F., Vrager A. and Leckner B., 1999, "Solids flow pattern in the exit region of a CFB-furnace-influence of exit geometry", 15th Int. Conf. on Fluidised Bed combustion, Savannah.

Kuipers J. A. M., Van Swaaij W. P. M., 1999, "Simulation of three-dimensional (3D) riser flow using kinetic theory of granular flow", In Werther J. (Ed.). 6th International conference on Circulating Fluidized Beds, W¨urzburg, Germany. 267-273.

Launder B. E., 1989, "Second-Moment Closure: Present and Future", Inter. J. Heat Fluid Flow, 10(4):282-300.

Launder B. E., Reece G. J., and Rodi W., 1975, "Progress in the Development of a Reynolds-Stress Turbulence Closure", J. Fluid Mech., 68(3):537-566.

Luben C. G., Fernando E. M., 2001, "Gas-Solid Two-Phase Flow in the Riser of Circulating Fluidized Beds: Mathematical Modeling and Numerical Simulation", J. Braz. Soc. Mech. Sci. Vol.23, no.2, Rio de Janeiro.

Lumley J., 1978, "Computational Modeling of Turbulent Flows", Adv. Appl. Mech., 18, 123.

Lun C. K. K., Savage S. B., Jeffrey D. J. and Chepurniy N., 1984, "Kinetic Theories for Granular Flow: Inelastic Particles in Couette Flow and Slightly Inelastic Particles in a General Flow Field", J. Fluid Mech., 140:223-256.

Lun C. K. K., Savage S. B., Jeffrey D. J. and Chepurniy N., 1984, "Kinetic theories for granular flow: inelastic particles in couette flow and slightly inelastic particles in a general flowfield", J. Fluid Mech. 140, 223–256.

Mathiesen V., Solberg T., Hjertager B. H., 1999, "A numerical study of three-dimensional multiphase flow pattern in a riser". In Werther J. (Ed.). 6th International Conference on Circulating Fluidized Beds, Wurzburg, Germany. 249-254.

Mathiesen V., Solberg T., Hjertager B. H., 2000, "An experimental and computational study of multiphase flow behavior in a circulating fluidized bed" Int. J. Multiphase flow, 26. 387-419.

Mathiesen V., 1997, "An experimental and computational study of multiphase flow behavior in circulating fluidized beds", PhD thesis. Telemark Institute of Technology (HiT-TF), Porsgrunn, Norway.

Miller A. and Gidaspow D., 1992, "Dense, vertical gas-solid flow in a pipe", AIChE J. 38(11), 1801–1815.

Morsi S. A. and Alexander A. J., 1972, "An Investigation of Particle Trajectories in Two-Phase Flow System", J. Fluid Mech., 55(2):193-208.

Neri A., and Gidaspow D., 2000, "Riser hydrodynamics: simulation using kinetic theory", AIChE J. 46(1), 52–67.

Nieuwland J. J., Meijer R., Kuipers J. A. M. and Van Swaaij W. P. M., 1996, "Measurements of solids concentration and axial solids velocity in gas-solid two-phase flows", Powder Technology 87, 127–139.

Patankar S. V., 1980, "Numerical Heat Transfer and Fluid Flow", Hemisphere, Washington D.C.

Patureaux T. and Barthod D., 2000, "Usage of CFD Modeling for Improving an FCC Riser Operation, Oil & Gas Science and Technology – Rev. IFP", Vol. 55, no. 2, pp. 219-225.

Peirano E., Leckner, B., 2000, "A mean diameter for numerical computations of polydispersed gas-solid suspensions in fluidization", Chem. Eng. Sci. 55. 1189-1192.

Peirano E., 1996, "The Eulerian/Eulerian formulation applied to gas-solid flows", Report A96-218, Department of Energy Conversion, Chalmers University of Technology, Sweden.

Petty C.A., Parks S.M., Weispfennig K., 1997, "An Algebraic preclosure theory for the Reynolds stress", Physics of fluids, Vol. 10, no. 3, pp. 645-653.

Pita J. A. and Sundaresan S., 1991, "Gas-solid flow in vertical tubes", AIChE J. 37(7), 1009–1018.

Ranade V. V., 1999, "Modeling of Gas-Solid Flows in FCC Riser Reactors: Fully Developed Flow", Second International Conference on CFD in Minerals and Process Industries, CSIRO, Melbourne, Australia.

Samuelsberg A. and Hjertager B. H., 1996, "An experimental and numerical study of flow patterns in a circulating fluidized bed reactor", Int. J. Multiphase Flow 22(3), 575–591.

Samuelsberg A. and Hjertager B. H., 1996, "Computational modeling of gas/particle flow in a riser", AIChE J. 42(6), 1536–1546.

Schiller L. and Naumann Z., 1935, Z. Ver. Deutsch. Ing., 77:318.

Shih T.-H., Liou W. W., Shabbir A., Yang Z. and Zhu J., 1995, "A New k -ε Eddy-Viscosity Model for High Reynolds Number Turbulent Flows - Model Development and Validation", Computers Fluids, 24(3):227-238.

Spalart P. and Allmaras S. 1992, "A one-equation turbulence model for aerodynamic flows", Technical Report AIAA-92-0439, American Institute of Aeronautics and Astronautics.

Stephen B. P., 2000, "Turbulent flows", Cambridge University Press, New York.

Sun B. and Gidaspow D, 1999, "Computation of circulating fluidized-bed riser flow for the fluidization viii benchmark test", Ind. Eng. Chem. Res. 38, 787–792.

Syamlal M., Rogers W. and O'Brien T. J., 1993, "MFIX Documentation: Volume 1, Theory Guide", National Technical Information Service, Springfield, VA, DOE/METC-9411004, NTIS/DE9400087.

Syamlal M., 1998, "High order discretization for the numerical simulation of fluidized beds", AIChE Symp. Ser. 94(318), 53–57.

Van den Moortel T., Santini L., Tadrist L. and Pantaloni J., 1997, "Experimental study of the particle flow in a circulating fluidized bed using a phase Doppler particle analyser: A new post-processing data algorithm", Int. J. Multiphase Flow 23(6), 1189–1209.

Van Wachem B. G. M., Van der Schaaf J., Schouten J. C., Krishna R. and Van den Bleek C. M., 2001, "Experimental validation of lagrangian-eulerian simulations of fluidized beds", Powder Technology 166, 155–165.

Wang T., Liu Z. J., Zhu C. M. , Liu D. C. and Saxena S. C., 1993, "Particle velocity measurements in a circulating fluidized bed" AIChE J. 39(8), 1406–1411.

Wang Y., Fei W. W., Yong J. and Zhiqing Y., 1998, "Radial profiles of solids concentration and velocity in a very fine particle riser" Powder Technology 96, 262–266.

Wen C. Y. and Yu Y. H., 1966, "Mechanics of Fluidization", Chem. Eng. Prog. Symp. Series, 62:100-111.

Werther, J., Hage B. and Rudnick C., 1996, "A comparison of laser Doppler and single-fibre reflection probes for the measurements of the velocity of solids in a gas-solid circulating fluidized bed", Chem. Eng. Proc. 35, 381–391.

Wilcox D. C., 1998, "Turbulence Modeling for CFD", DCW Industries, Inc., La Canada, California.

Yang, Y.L., Jin Y., Yu Z. Q., Zhu J. X. and Bi H. T., 1993, "Local slip behaviours in the circulating fluidized bed", AIChE Symp. Ser. 89, 81–90.

Zhang, Wennan, Filip J. and Leckner B., 1995, "Fluid-dynamic boundary layers in CFB boilers", Chem. Eng. Sci. 50(2), 201–210.

Zhang, Yu-Feng and Arastoopour H., 1995, "Dilute fluidized cracking catalyst particles-gas flow behaviour in the riser of a circulating fluidized bed", Powder Technology 84, 221–229.

Zhang D. Z., VanderHeyden W. B., 2001, "High-resolution three-dimensional numerical simulation of a circulating fluidized bed", Powder Technology. 116. 133-141.

Zhou, Haosheng, Jidong L. and Liang L., 2000, "Turbulence structure of the solid phase in transition region of a circulating fluidized bed", Chem. Eng. Sci. 55, 839–847.